Full length article

Tectonically controlled evolution of the Yellow River drainage system in the Weihe region, North China: Constraints from sedimentation, mineralogy and geochemistry

Jin Liu[a,b], Xingqiang Chen[c,d,*], Wei Shi[d], Peng Chen[d], Yu Zhang[a], Jianmin Hu[d], Shuwen Dong[e], Tingdong Li[b]

[a] Scholl of Civil and Architecture Engineering, Xi'an Technological University, Xi'an 710021, China
[b] Institute of Geology, Chinese Academy of Geological Sciences, Beijing 100037, China
[c] China Railway First Survey & Design Institute Group CO., LTD., Xi'an 710043, China
[d] Institute of Geomechanics, Chinese Academy of Geological Sciences, Beijing 100037, China
[e] School of Earth Science and Engineering, Nanjing University, Nanjing 210093, China

ARTICLE INFO

ABSTRACT

This study investigated the evolution of the middle reach of the Yellow River by examining the latest Cenozoic (~5.0–0.15 Ma) sedimentary history of the Weihe and Sanmenxia basins in the Weihe region of North China. Although the development of the two basins and the evolution of the Yellow River have long been related to the rapid uplift of the Tibetan Plateau, the relationship between the landform evolution and regional tectonics is still poorly understood. Here, we report the results of a detailed study on sedimentation and provenance of the two basins and their spatial and temporal relationships to regional fault development. The results show that the two basins were possibly originally isolated from each other, between ~5 Ma and ~2.8–2.6 Ma, but later connected by the Yellow River at ~2.8–2.6 Ma. This process is recorded in the coarsening-upward sequence of the Weihe Basin strata and the coeval fining-upward succession of the Sanmenxia Basin strata. At ~1.0 Ma, the Sanmenxia Basin strata developed a coarsening-upward trend, which we interpret as an indication of the formation of the Yellow River in the region. In addition, changes in the drainage system at ~2.8–2.6 Ma and at ~1.0 Ma have been recorded as dramatic provenance changes in the sediments of the Sanmenxia Basin.

1. Introduction

Understanding how continental landforms have evolved is of great importance because it provides key information on the interactions between tectonic deformation of the lithosphere, climate change, and surface processes (Hamidullah et al., 2001; Zhang et al., 2016). Rapid uplift and the northeastward extrusion of the Tibetan Plateau (Fig. 1a), which was one of the most important tectonic-geomorphic events in eastern Asia during the Cenozoic, led to the formation of a series of landforms in and around the plateau (Molnar and Tapponnier, 1975; Tapponnier et al., 1982; An et al., 2001; Yin, 2010). The fault systems, half-graben basins (Weihe and Sanmenxia basins), and drainage systems (Yellow River) in the Weihe region (Fig. 1b and c), North China, have long been related to the tectonic evolution of this plateau (Peltzer et al., 1985; Tapponnier et al., 1986; Zhang et al., 1998, 2003; Sun, 2005; Yin, 2010; Hu et al., 2017). Because of the difficulty in dating the

brittle fracturing that controlled the formation of the landform (Zhang et al., 2003; Shi et al., 2015), the exact transition timing and pattern of regional stress still lacks proper understanding. This uncertainty has prevented the understanding of the relationship between the evolution of the landforms and the regional tectonics.

Examining sedimentary facies and provenance records of the tectonically controlled basins and drainage systems could be an effective way to address this issue. Most paleolakes existed before the Yellow River connected them within the modern drainage systems (Dai, 1983; Zhang, 1987; Zhu, 1989; Craddock et al., 2010), thereby having different sedimentary environments and source areas, but be related thereafter. Additionally, the source rocks in the Weihe region are spatially distinct in composition (Fig. 1c), indicating that provenance analysis could be a suitable method to study their erosion and sediment transport history (Clark et al., 2004; Clift, 2006; Zhang et al., 2016). Therefore, by analyzing the latest Cenozoic (~5.0–0.15 Ma)
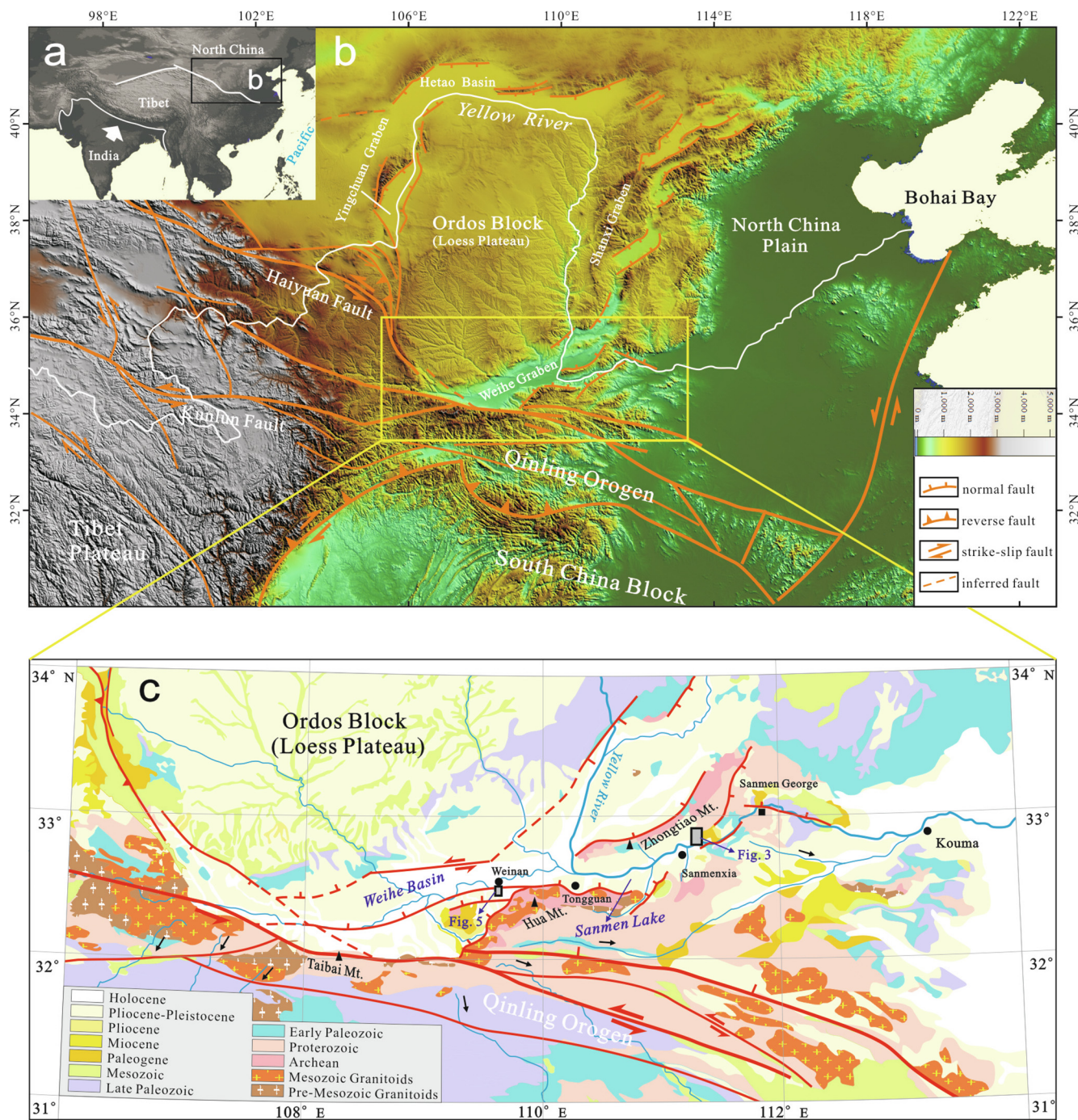
Fig. 1. (a) and (b) Simplified structural map of the study area and its adjacent area based on Digital elevation model (DEM, from https://wist.echo.nasa.gov/wist-bin/api/ims.cgi?mode=MAINSRCH&JS=1) showing the location of the Sanmenxia Basin and the Weihe basin. The structural map is modified from Zhang et al. (2003) and Shi et al. (2015). (c) Geological map of the Sanmenxia Basin and the Weihe Basin. Lithology of different strata is presented in the text.

sedimentary history of the basins based on sedimentation, detrital heavy minerals and geochemical analyses, we investigate the evolution of the Yellow River, and discuss their influence on the timing and pattern of the latest stage of the plateau uplift.

2. Geological setting

The Yellow River is the second longest river in China, with a length of 5464 km, and an elevation variation of more than 4 km from its source in the Tibetan Plateau to where the river enters the Pacific Ocean at the Bohai Sea (Fig. 1a and b). The river cuts through a young valley in the Quaternary eolian loess deposits along the western front of

the Lvliang Mountain and flows southward into the Weihe Basin in the northernmost Weihe Graben. Turning eastward at the Tongguan County, the river flows due southeast through the Sanmenxia Basin and then due east through the Sanmen Gorge before reaching the North China Plain at Kouma village.

Both the Weihe and Sanmenxia basins are NE-SW elongate depo-centers mainly bounded by the northeast-striking, northwest-dipping normal faults (Zhang et al., 2003). Some northwest-striking faults developed between the basins and in the Sanmen Gorge. The Weihe Basin is located between the active Qinling orogenic belt in the south and the relatively stable Ordos Block in the north, whereas the Sanmenxia Basin is located north of the Qinling Orogen and south of the Zhongtiao

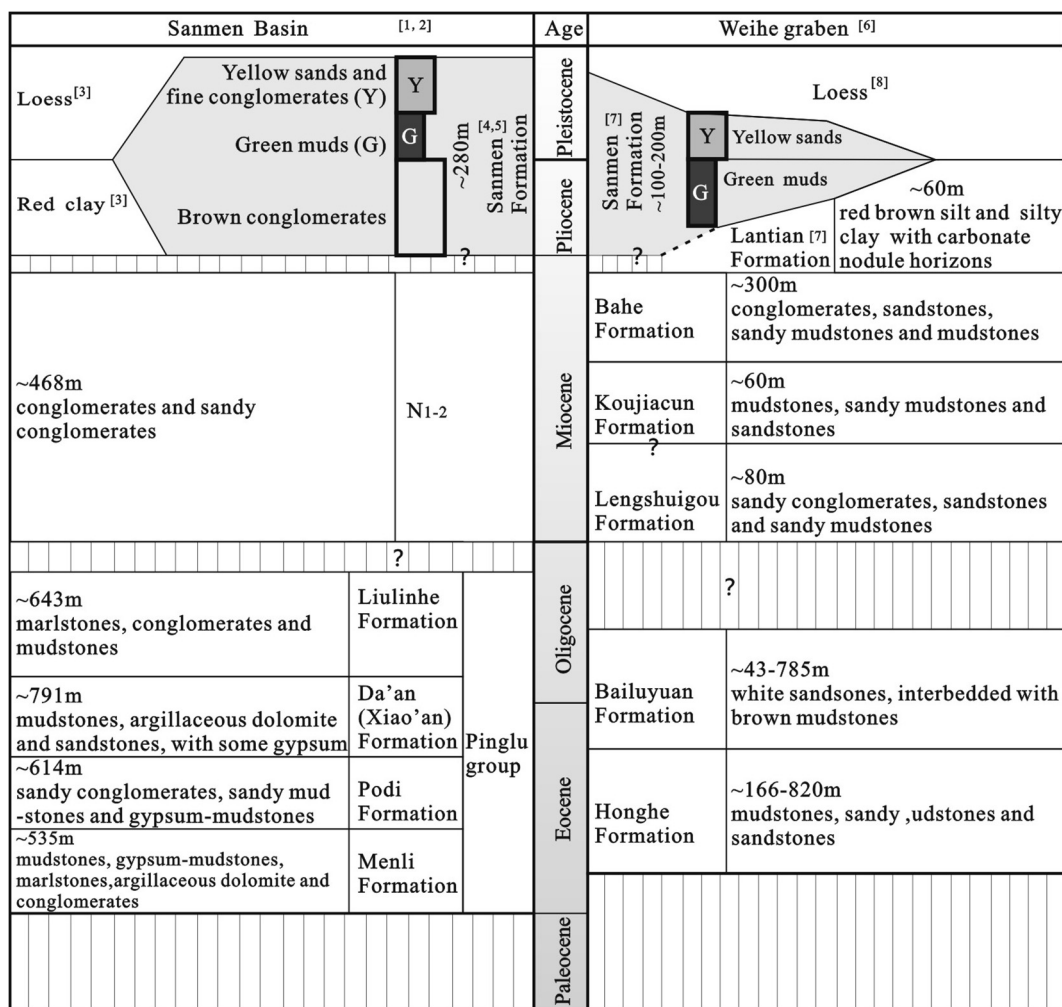| Sanmen Basin [1,2]		Age	Weihe graben [6]	
Loess[3]; Yellow sands and fine conglomerates (Y) [Y]; Green muds (G) [G]; Red clay[3]; Brown conglomerates	~280m [4,5] Sanmen Formation	Pleistocene / Pliocene	Sanmen Formation[7] ~100-200m, Yellow sands [Y], Green muds [G]; Loess[8]; Lantian[7] Formation	~60m red brown silt and silty clay with carbonate nodule horizons
~468m conglomerates and sandy conglomerates	N1-2	Miocene	Bahe Formation	~300m conglomerates, sandstones, sandy mudstones and mudstones
			Koujiacun Formation	~60m mudstones, sandy mudstones and sandstones
			Lengshuigou Formation	~80m sandy conglomerates, sandstones and sandy mudstones
~643m marlstones, conglomerates and mudstones	Liulinhe Formation	Oligocene	Bailuyuan Formation	~43-785m white sandsones, interbedded with brown mudstones
~791m mudstones, argillaceous dolomite and sandstones, with some gypsum	Da'an (Xiao'an) Formation — Pinglu group			
~614m sandy conglomerates, sandy mud-stones and gypsum-mudstones	Podi Formation	Eocene	Honghe Formation	~166-820m mudstones, sandy ,udstones and sandstones
~535m mudstones, gypsum-mudstones, marlstones, argillaceous dolomite and conglomerates	Menli Formation	Paleocene		

Fig. 2. General stratigraphy of the Sanmenxia Basin and the Weihe basin. References: 1 is from Wang and Chen (2005); 2 is from SBGMR (1989a); 3 is from Zhao et al. (2006); 4 is from Wang et al. (1999); 5 from is Jiang et al. (2007); 6 is from SBGMR (1989b); 7 from is Hu et al. (1993); and 8 is from Wang et al. (2014).

Mountain (Fig. 1b and c). The eastern part of the Qinling Orogen (Hua and Taibai Mountains) is mainly composed of granitoids (Pre-Mesozoic and Mesozoic) and metamorphic rocks (Archean and Lower Proterozoic), while the western part of the orogen is composed of sedimentary rocks (Upper Proterozoic). The Ordos Block, however, consists mainly of Paleozoic and Mesozoic sedimentary rocks (sandstone and mudstone, with minor limestone) (Fig. 1c). Further, the Zhongtiao Mountain exposes both Archean metamorphic rocks on the northern part, and Upper Proterozoic to Paleozoic sedimentary rocks on the eastern part.

The Pliocene-Pleistocene sediments of both the basins are represented by the fluvio-lacustrine Sanmen Formation and the overlying eolian loess (Wang et al., 2013). The Sanmen Formation is overlain by the Pinglu Group in the Sanmenxia Basin (Wang and Chen, 2005) and the Bahe Formation in the Weihe Basin (SBGMR, 1989). The entire pre-Pliocene Cenozoic succession in the Sanmenxia Basin is divided, in chronological order from bottom to top, into the Menli, Podi, Da'an, and Liulinhe formations and conglomerates of the Neogene age (SBGMR, 1989; Wang and Chen, 2005). In the Weihe Basin, the succession comprises of the Honghe, Bailuyuan, Lengshuigou, Koujiacun, and Bahe formations (Fig. 2).

3. Study area and methods

Fieldwork in the Sanmenxia Basin mainly focused on outcrops along the Huangdigou River (Figs. 1c, 3, and 4). The exposures provided a favorable opportunity for detailed sedimentological study of the Sanmen Formation. Along the river from north to south, a total of nine vertical sections within a distance of ~6 km (collectively called the Huangdigou section, i.e., from 111°16′54″ to 111°16′56″ E and 34°49′38″ to 34°49′48″ N) were logged and measured. Individual sections were subsequently correlated by tracing marker horizons (like conglomerate layers). Five of these vertical sections yielded paleomagnetic ages of ~5.0 Ma (Wang et al., 1999). In the Weihe Basin, a vertical section with an age of ~3.15 Ma on the bottom (Hu et al., 1993), known as the Songjiabeigou section (Figs. 1c and 5, 109°30′43″ E and 34°25′53″ N) on the west bund of the Youhe River, was investigated. This section contains the middle-upper part of the Sanmen Formation.

Following the facies coding scheme originally introduced by Miall and Gibling (1978) and Miall (1984, 1985), 13 types of lithofacies (Table 1) and 4 facies associations (Table 2) were distinguished within the sediments. Additionally, sediment samples were collected from each representative layer of units 1–4 of the Huangdigou section for detrital heavy mineral and geochemical analyses, and investigation of the paleocurrent indicators and clasts components are carefully examined. These methods for examining provenance are available in detail in Li et al. (2014), Zhu et al. (2017), Liu et al. (2018), and Peng et al. (2018). Care was taken when collecting the samples, to avoid weathering, hydrothermal alteration, and mineralization influence. Thin sections were prepared for each sandstone sample, which were point-counted for Q-F-L plotting following the Gazzi–Dickinson method (Dickinson, 1983). Major element oxides and trace elements, including 14 rare earth

Table 1
Facies codes, lithofacies characteristics, sedimentary structures, and interpretations of the Sanmen Fm, modified from Miall and Gibling (1978) and Miall (1984).

Codes	Lithofacies	Sedimentary structures	Interpretation
Gm	Massive, matrix supported gravel	Imbricate clasts, or massive	Debris-flow deposits
Gl	Thin-stratified or lens-shaped, matrix or grain supported gravel	Grading or massive	Minor channel fills
St	Sand, medium to coarse, may be pebbly	Trough cross-bedding, scour structures	Dunes
Sp	Sand, medium to coarse, may be pebbly	Small-scale planar cross-bedding	Linguoid sandy bars
Ss	Sand, medium to coarse, may be pebbly	Massive	Grain flow deposits
Sh	Sand, very fine to coarse	Horizontal bedding	Low energy and flows
Sr	Sand, very fine to coarse	Ripple marks of all types	Unstable flows/ ripples
Sds	Inter-beds of silt, clayey silt, sandy mud, and mud.	Horizontal bedding	Seasonal flows, flood plains
Fm	Mud, silt	Massive, desiccation cracks	Overbank or lake
Fl	Mud mix with silt and sands	Fine lamination to massive, may with very small ripples	Overbank, waning flood deposits, or lake
Fsc	Silt, mud	Laminated to massive	Back swamp deposits or lake
Frc	Red clay, with lithite	Massive	Eolian
Fym	Yellow- brownish silts/mud, may with lithite	Massive	Eolian

Table 2
Facies associations of the investigated sections. Elements are modified from Miall (1985). See Table 1 for explanation of the lithofacies.

| Facies	Sub-facies	Elements (lithofacies)
Alluvial Fan	Upper fan (UP)	Gm-Ss, Gm-Fl, Frc
	Inner fan (IP)	Gl-Ss, Gl-Fl, Frc
	Lower fan (LF)	Gl, Ss, Fl
Lacustrine	Shore lake	Fl, Fsc, Ss, Sh, Sp, Sr, Gl
	Shallow lake	Fsc, Sds, Ss, Sh, Sp, Sr, Fl, Fm
	Deep lake	Fsc, Fl, Fm
Fluvial	Bedform lag deposits (BLD)	Gl
	Distributary channel (DC)	Ss, St, Sp
	Natural levees (NL)	Sh, Sr
	Flood plain (FP)	Sh, Ss, Fl
Aeolian	Loess	Fym

elements (REE), were analyzed by standard X-ray fluorescence (XRF) and inductively coupled plasma mass spectrometry (ICP-MS) techniques, respectively at the Analytical Laboratory, Beijing Research Institute of Uranium Geology. Precision and accuracy for major elements were within 1%. Accuracy for the trace and rare earth elements were better than 10% for all analyzed elements.

4. Results

4.1. Sedimentation of the basins

4.1.1. Sedimentation of the Huangdigou section in Sanmenxia Basin

The sub-sections of the Huangdigou section (Pm01, Pm02, Pm05, Pm06, Pm07, Pm08, and Pm09 in Fig. 3) consist mainly of gray conglomerates, yellowish sands, green or yellowish mud, and minor yellow
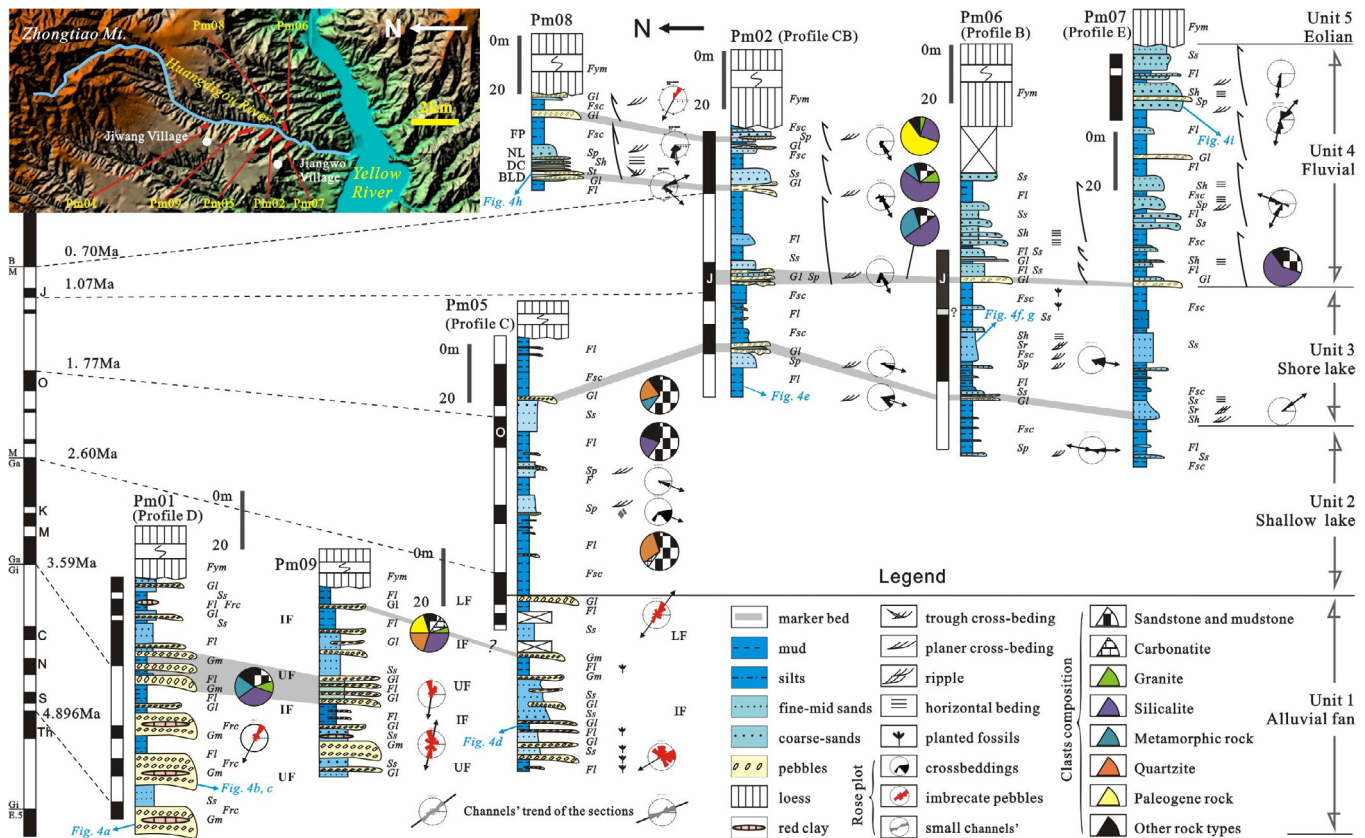
Fig. 3. Sedimentation of Huangdigou profile (GPTS is from Gradstein et al. (2012); and the magnetostratigraphic ages is followed Wang et al. (1999); Pm06 was revised based on the field correlation of the sections. See Tables 1 and 2 for explanation of the abbreviations of the facies codes (i.e. Fym, Gl, Ss, etc) and facies associations (i.e. FP, NL, DC, BLD, etc.), respectively.
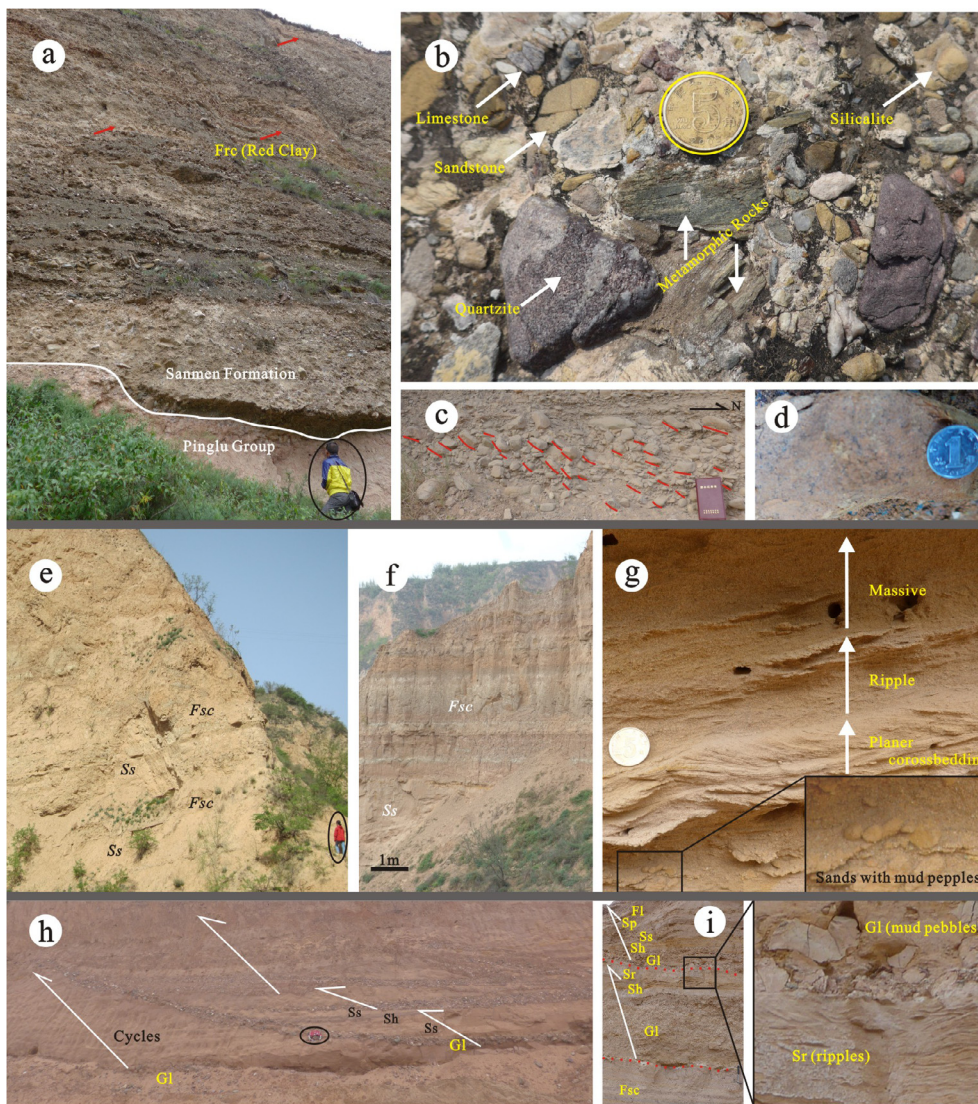
Fig. 4. Field photographs of the Huangdigou sections in Sanmenxia Basin. See Table 1 for explanation of the abbreviations of the facies codes (i.e. Fym, Gl, Ss, etc.). (a) Thick conglomerate layers (Gm) in unit 1 with some lens sands, mud and red clay (Frc) layers, where we can find the unconformity between the Sanmen Formation and the underlay Pinglu Group. The man is about 1.7 m high in scale; (b) Some kinds of clasts in the unit 1, most of which are clast-supported, poorly sorted, sub angular round with a diameter of 1–5 cm. The coin is about 1.5 cm wild in scale; (c) Imbricate clast in unit 1, showing a southern direction of the flows. The book is about 20 cm long in scale; (d) Yellow mud sands with charcoal in unit 1. The coin is about 1.5 cm wild in scale; (e) Green mud layers (Fsc) with some yellowish colored sands (Ss) in unit 2, showing an oxygen-free circumstance of shallow lake. (f) Alternating layers of green mud (Fsc) and yellow sands (Ss) in unit 3, showing a lakeshore environment; (g) Yellow sands with small planer cross-beddings, ripples and horizontal beddings in unit 3, showing a turbulent environment of lakeshore. The coin is about 1.5 cm wild in scale; (h) and (i) Cycles from bedform lag deposits (Gl) to distributary channel (Ss, Sp) and natural levees (Sh, Sr), then to flood plain (Fl, Ss) in unit 4, showing the morphology of the fluvial. The bag and the hammer are about 30 cm wild and 30 cm long in scale, respectively. (For interpretation of the references to colour in this figure legend, the reader is referred to the web version of this article.)

silt. Five distinct sequences were recognized: an alluvial fan in unit 1, a shallow lake in unit 2, a lake shore environment in unit 3, a fluvial setting in unit 4, and eolian loess in unit 5.

Unit 1 (~5 to 2.8–2.6 Ma) is characterized by fining- and thinning-upward conglomerates and sands with minor mud (Fig. 3). Almost all the sediments are poorly sorted, sub-angular to moderately rounded, and comprise a lithofacies association mainly of Gm, Gl, Ss, Fl, and Frc (Fig. 4a and b). Imbricate clasts (Fig. 4c) and charcoal (Fig. 4d) are common, whereas fossils are rare. The bottom, middle, and upper layers of the sediments, all dipped towards the south, except at different angles, i.e., at typically ~10° for the first layer, and at 5°–10° for the other two layers. The oxidized nature, low maturity, and hydraulic characteristics of the sediments indicated that this unit was deposited in an alluvial-fan environment (Scholle and Spearing, 1982). Three sub-facies (upper, inner, and lower fans) were recognized in the outcrop. The upper-fan association is characterized by conglomerates (Gm and a few Gl, with clast diameters of 2–5 cm or larger, making up a maximum of 70% of the rock mass), with small amounts of yellow sand, silt, and mud (Ss, Fl, and Frc). The conglomerate layers are often massive or with imbricate clasts, with development of some graded bedding in the sand layers (Fig. 4a). The most significant feature of the inner-fan deposits is the presence of half-cycle braided channel sediments that show a fining-upward trend with part of the lithofacies of a braided channel cycle. The lithofacies association of Gl, Ss, and Fr (Fig. 3) indicates a

transitional sedimentary environment between the lower and upper fans. The grain size in the inner fan is finer, and sediments are more mature than in the upper fan. The lower-fan sediments consist mainly of the Ss and Fm lithofacies, which were deposited in a low-energy environment.

Unit 2 (~2.6–1.8 Ma) was deposited in shallow lake subfacies, and consists of green- and gray-colored thick mud, silt layers (Fig. 4e), and some sand veins or lenses with fine clasts. This subfacies contains a lithofacies association of Frc, Ss, Sh and Sp, with minor Fl and Fm. Although horizontal bedding occurs widely, with some trough cross-bedding, most of the sediments are massive, suggesting a relatively stable sedimentary environment (shallow lake).

Unit 3 (~1.8–1.0 Ma), deposited in lakeshore subfacies, mainly consists of yellow mudstone with intercalated mud to medium sand and silt, within conglomerate lenses in the sand layers. This unit contains a lithofacies association of Fl, Fsc, Ss, Sh, Sp, and Sr, with minor Gl. A greater variety of sedimentary structures were observed in the lakeshore subfacies than in the shallow lake facies, including horizontal lamination, horizontal bedding, wave bedding, and small planar cross-bedding. The presence of bioturbation indicates an oxygenated environment. The Gl lithofacies at the base of this unit does not appear in most lake environments, and may indicate the occurrence of sediment gravity flows (i.e., turbidity currents).

Unit 4 (~1.0–0.15 Ma) consists of multiple cycles of fining-upward
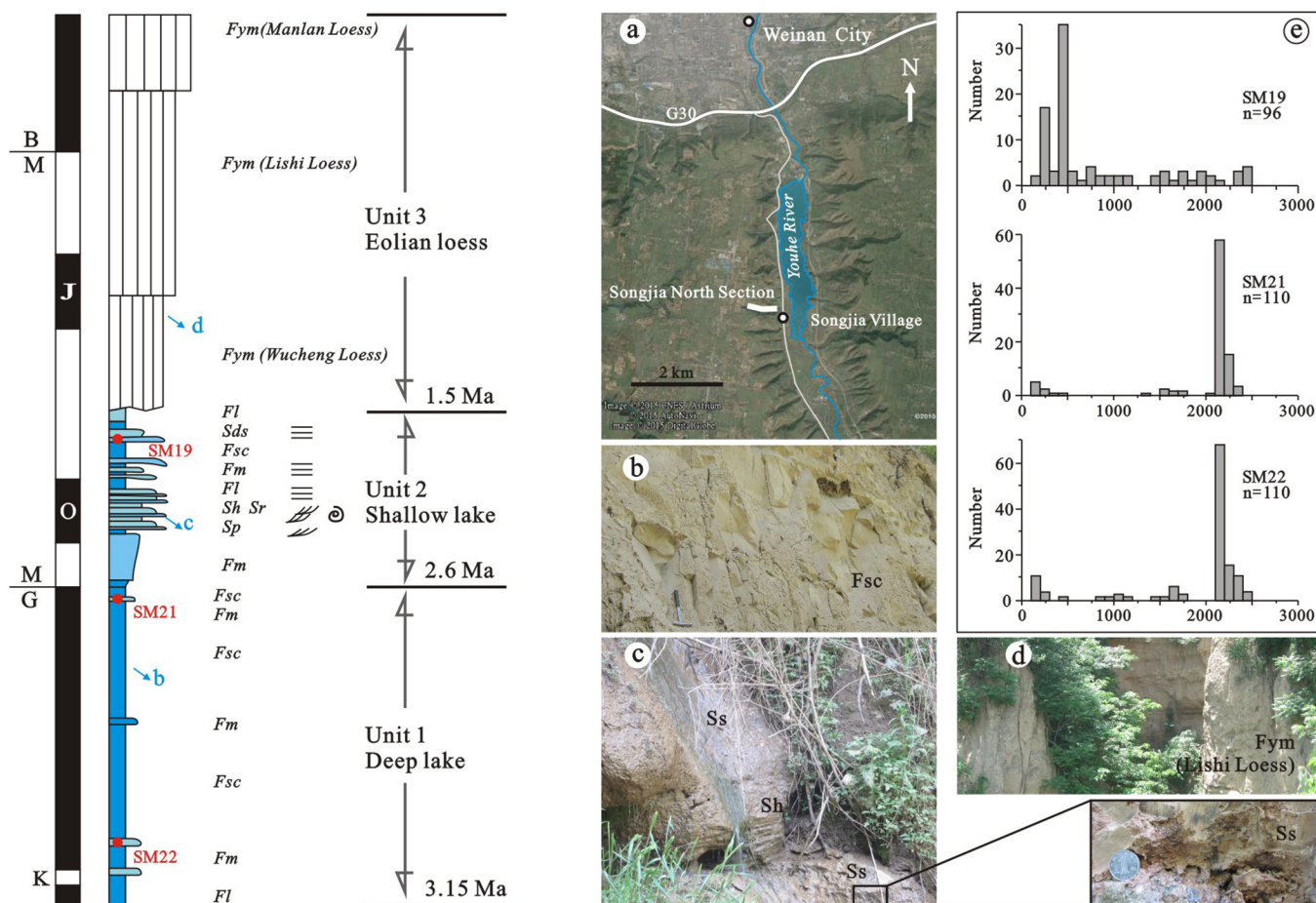
Fig. 5. Sedimentation and the outcrop photographs of the Songjiabeigou section; and the magnetostratigraphic ages are modified from Hu et al. (1993). See Table 1 for explanation of the abbreviations of the facies codes (i.e. Fym, Fl, Sds, etc.). (a) ERDAS map from Google earth, showing the location of the Songjiabeigou section; (b) Gray colored mud (Fsc) in unit 1. The hammer is about 30 cm in scale; (c) Massive coarse sands (Ss) with horizontal beddings (Sh) in unit 2, where charcoal can be found. (d) Aeolian Loess (Fym; Lishi Loess) composed of light yellow mud silts in unit 3. (e) Zircon U-Pb age distributions in the Songjiabeigou section (from Kong et al., 2014).

brown/dark-gray conglomerates at the bottom, yellowish/green sands in the middle, and mud in the upper part, given which it could be interpreted as a fluvial setting. Multiple types of sedimentary structures were developed in this unit, with planar cross-bedding, trough cross-bedding and parallel bedding being the most abundant. The oxidized nature and hydraulic characteristics indicate a fluvial depositional environment (Allen, 1970; Cant and Walker, 1976) that was much more unstable than the lacustrine environment. Some mammalian fossils were also found. The lower part of the section exhibited Youhe fauna (including Stegodon sp., and Cervavitus sp.), and is comparable to the Dongyaozitou fauna in the Nihewan Basin, belonging to the Pliocene age (Hu et al., 1994). The upper part of the section contains *Lynx* cf. *shansius, Rusa elegens, Gagalla* sp., *Hipparion* sp., *Bovinae, Eguus sanmeniensis, Rhinocerotidae* sp. etc., aged between the Nihewan fauna and Yangguo fauna, belonging to the early Pleistocene. The lower part of the section is plentiful in *Ilyocypris-Candona* and *Ilyocypris-Candoniella* assemblages, while the upper part is characterized by *Lineocypris-Lishania* assemblage (Wang et al., 2010), the boundary being consistent with the boundary obtained from the paleomagnetic studies (Hu et al., 1993; Yue and Xue, 1996). The mammalian fossils and ostracoda results affirm the reliability of paleomagnetic dating. At least four micro-facies have been identified that form a fining-upward cycle. From base to top, these are bedform lag deposits, distributary channels, natural levees, and flood plains (Table 2 and Fig. 3).

Unit 5 (younger than ∼ 0.15 Ma) is mainly composed of eolian loess that unconformably overlies unit 1 to 4 in all the sections. The Lishi

loess (light yellow muddy silts) was deposited in some older sections, while the Malan loess (gray-yellow silts) was observed in all the outcrops. Wang et al. (1999) obtained two TL dates in the loess and lacustrine sediments, having ages of 100.5 ± 7 ka and 251.8 ± 23 ka in pm07 section, respectively. These results are consistent with the dates obtained from paleomagnetic studies.

Provenance from paleocurrent and clasts composition: The orientations of cross-bedding and imbricate clasts indicate that the paleocurrents changed from unit 1 to unit 4 in the sections (Fig. 3), signifying that the source areas of the sections were changed. In unit 1, between ∼ 5 and ∼ 2.8–2.6 Ma, the paleocurrents were mostly directed towards the south, while the trends of the scour troughs of the smaller channels indicate a consistent direction. However, in units 2 and 3, between ∼ 2.6 and ∼ 1.0 Ma, the paleocurrents were directed mainly to the east. In unit 4, the paleocurrents appear more disordered than in unit 1 to 3, but with a dominant direction to the south and southwest at ∼ 1.0–0.15 Ma.

The compositions of the clasts in different conglomerates also varied across different units (Fig. 3). The clasts in unit 1 are mainly sedimentary rocks of sandstone and limestone, while units 2 and 3 consist solely of sandstones. In unit 4, magmatic (granitoid and silicolite) and metamorphic (schist, slate and gneisses) rocks together make up more than 60% of the clasts. Additionally, the pebbles in units 1 and 4 are poorly sorted and coarse-grained (d = 5–0 cm), suggesting a nearby source, whereas moderately sorted and grained (d = 1–3 cm) clasts in units 2 and 3 may have come from a more distant area.
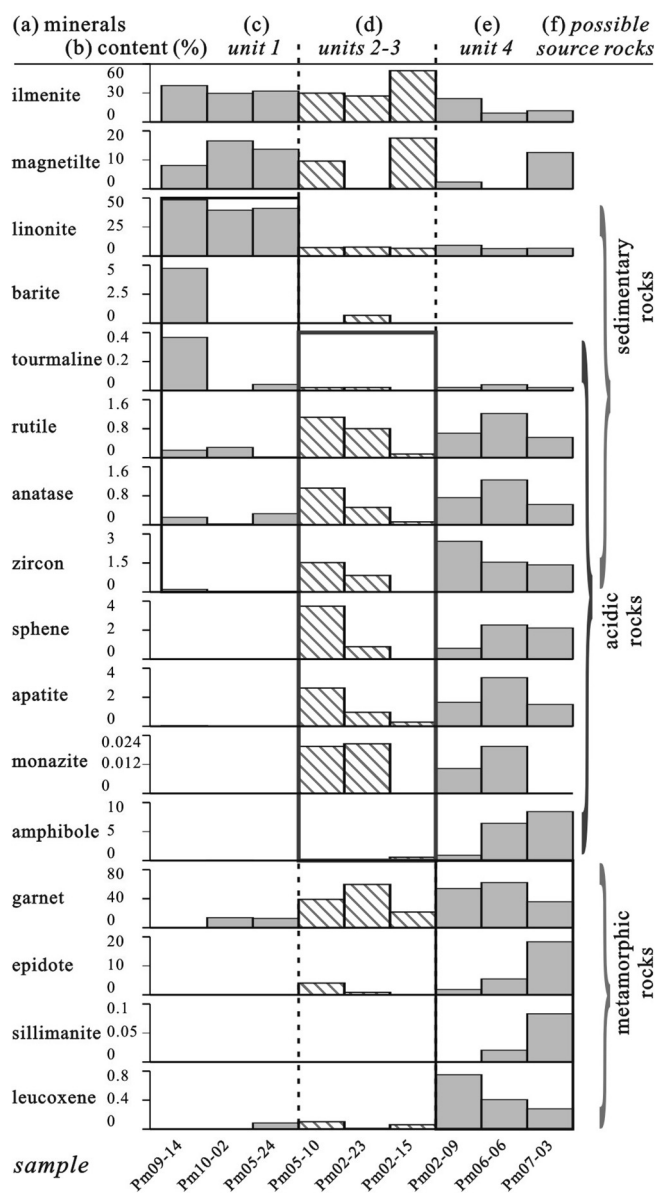
Fig. 6. Bar chart of the statistical detrital heavy minerals (DHM) from the Huangdigou section.
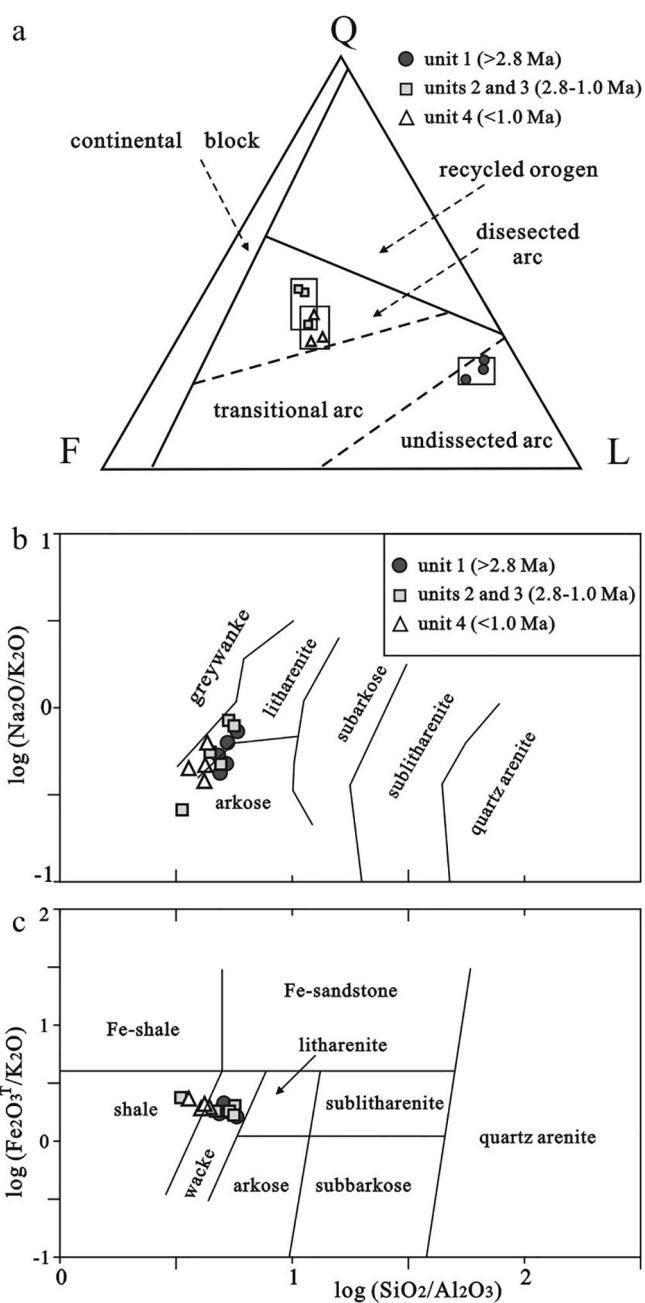

Fig. 7. (a) Q-F-L ternary diagrams (after Dickinson, 1983) of sandstone samples of the Huangdigou section. (b–c) Chemical classification diagram discriminating sediments of the Huangdigou section by their logarithmic ratios of (a) SiO_2/Al_2O_3 versus Na_2O/K_2O (after Pettijohn et al., 1987) and (b) Fe_2O_3T/K_2O (after Herron, 1988).

4.1.2. Sedimentation of the Songjiabeigou section in Weihe Basin

The Songjiabeigou section contains mainly yellowish sand, and green and blue clay. The section can be divided into three units: lacustrine sediments (deep lake) in the lower part, fluvial deposits in the middle, and eolian loess in the upper parts.

Unit 1 (prior ~2.6 Ma) of the Songjiabeigou section is characterized by gray-green mud, silt, and intercalated black thin- to medium-stratified sand, with the lithofacies association of Fsc, Fm, and Fl (Fig. 5b). Most of the silt and mud layers contain fossil ostracod assemblages, and some horizons are rich in calcium. The thicknesses of the differently colored mud and silt layers ranged between 1 and 3 m, while thickness of the sand layers was less than 0.3 m. Together, these characteristics indicate a deep lake subfacies.

Unit 2 (~2.6–1.5 Ma) mostly represents a shallow lake sedimentary environment. This unit contains a lithofacies association of Ss, Fsc, Sds, Fl, Sp, Sh, Sr, and Fm, consisting mainly of yellowish, massive thick and thin mud and sand layers, with a few thin sand layers. Cross-bedding is rare (Fig. 5c), suggesting a low-energy environment or a scarce sediment supply.

Unit 3 (younger than ~1.5 Ma) is composed mainly of eolian loess

(Fig. 5d) that unconformably overlies units 1–2. The loess can be subdivided into the Wucheng Loess (brown silty mud), the Lishi Loess (light yellow muddy silts), and the Malan Loess (gray-yellow silt), from bottom to top.

4.2. Mineralogy of the Huangdigou section

Based on the petrographic work (thin sections), the sandstones samples were subdivided into two distinct petrofacies: feldspathic litharenite dominated in unit 1, and lithic arkose in units 2, 3, and 4. The feldspathic litharenite was mainly rock clasts and feldspars, with less than 25% quartz. However, the sediments in this group also contained significant amounts of calcite and/or dolomite. The lithic arkose group

Table 3
Major element concentrations (wt%) for silts and mud of the Huangdigou section.

Unit	Unit 1					Units 2–3				Unit 4				
Sample	Pm 01–6	Pm 09–4	Pm 05–24	Pm 05–22	Pm 05–20	Pm 05–13	Pm 05–9	Pm 02–25	Pm 02–18	Pm 02–16	Pm 02–14	Pm 02–1	Pm 07–9	Pm 07–2
SiO_2	66.11	60.60	56.25	53.10	55.78	24.88	53.20	57.81	35.00	48.02	60.46	52.62	56.69	52.75
Al_2O_3	13.59	11.69	10.75	9.18	11.59	7.45	9.91	11.87	6.20	10.88	14.12	14.71	13.69	12.52
$Fe_2O_3{}^T$	5.72	5.76	4.11	3.11	4.51	3.30	3.35	4.94	2.74	4.65	6.22	6.37	4.95	5.07
MgO	2.64	3.54	4.16	4.34	4.99	11.26	1.83	3.06	10.96	4.67	3.33	3.70	3.14	4.22
CaO	0.63	4.62	7.52	11.22	6.04	20.57	13.41	6.64	16.30	11.28	2.28	5.99	6.38	8.06
Na_2O	1.24	1.30	1.33	1.41	1.27	0.36	1.63	1.27	1.04	1.34	1.82	1.27	1.01	1.14
K_2O	2.99	2.78	2.16	1.95	2.43	1.42	1.99	2.71	1.40	2.45	3.09	2.87	2.73	2.48
MnO	0.11	0.10	0.07	0.06	0.07	0.16	0.10	0.06	0.13	0.08	0.07	0.09	0.06	0.08
TiO_2	0.78	0.77	0.64	0.52	0.62	0.34	0.57	0.68	0.39	0.56	0.73	0.68	0.70	0.59
P_2O_5	0.06	0.10	0.07	0.07	0.07	0.08	0.12	0.12	0.08	0.18	0.13	0.16	0.15	0.13
LOI	5.70	8.68	12.54	14.73	12.39	30.12	13.53	10.40	25.69	15.40	7.39	11.28	10.50	12.84
FeO	0.84	0.55	0.87	0.81	0.73	0.51	1.03	0.79	0.93	0.78	1.30	1.07	1.40	0.98
SiO_2/ Al_2O_3	4.86	5.18	5.23	5.78	4.81	3.34	5.37	4.87	5.65	4.41	4.28	3.58	4.14	4.21
Na_2O /K_2O	0.41	0.47	0.62	0.72	0.52	0.25	0.82	0.47	0.74	0.55	0.59	0.44	0.37	0.46
$Fe_2O_3{}^T/K_2O$	1.91	2.07	1.90	1.59	1.86	2.32	1.68	1.82	1.96	1.90	2.01	2.22	1.81	2.04
Al_2O_3/TiO_2	17.38	15.14	16.85	17.59	18.57	22.17	17.51	17.59	16.06	19.33	19.32	21.73	19.67	21.08
K_2O/Na_2O	2.41	2.14	1.62	1.38	1.91	3.93	1.22	2.13	1.35	1.83	1.70	2.26	2.70	2.18

Note: LOI, loss on ignition.

Table 4
Trace element concentrations (ppm) for silts and mud of the Huangdigou section.

Unit	Unit 1					Units 2–3				Unit 4				
Sample	Pm 01–6	Pm 09–4	Pm 05–24	Pm 05–22	Pm 05–20	Pm 05–13	Pm 05–9	Pm 02–25	Pm 02–18	Pm 02–16	Pm 02–14	Pm 02–1	Pm 07–9	Pm 07–2
Li	34.7	26.7	26.7	22.7	34.1	34.5	25.5	28.5	18.6	30.9	28.9	51.5	48	55.1
Be	1.96	2.03	1.15	1.38	2.05	1.46	1.35	1.94	1.09	1.79	2.27	2.35	2.05	2.22
Sc	12.8	13.6	9.85	8.27	11	7.87	8.43	11.4	7.07	11.4	14.1	14.9	14.5	15.9
V	95.4	87.1	73.6	58.2	83.8	56.9	58.4	80.4	46.5	78.2	94.2	113	88.2	101
Cr	59	50.2	60.4	43.1	54.4	43.7	51.4	54.5	25.4	45.9	60.9	79.3	91.2	83.3
Co	16.7	17.3	10.1	8.62	12.3	10.7	9.97	13.2	8.36	12.2	14.6	16	15.4	14.3
Ni	29.7	24.9	27.6	23.3	26.8	27.7	24.7	27.4	18.1	25.8	26.4	39.5	41.2	37.6
Cu	34.3	33.1	23.6	18.4	27.8	19.8	21.4	29.4	17.3	27.8	29.3	37.8	27.9	74.5
Zn	79.5	69.1	61.7	48	66.9	54.1	52.3	68.5	44	80.5	113	97.2	80.9	114
Ga	17.7	14.4	12.7	10.6	14.7	9.76	12.1	15.1	7.88	14.1	18.3	18.4	16.4	16.6
Rb	108	102	82.5	67.9	93.7	56.6	74	101	49.3	95	120	119	104	98.6
Sr	129	146	275	367	352	871	230	183	1293	438	185	245	187	338
Y	21.9	24.3	24.4	19.8	22.4	13.7	21.6	23.7	13.1	21	22.6	25.1	23.1	24.6
Zr	185	214	153	137	160	59	126	159	66.7	111	135	113	126	120
Nb	15	13.3	12.9	10.5	13.5	6.68	11.5	13.3	6.31	10.6	11.2	13.7	13.8	13.2
Cs	6.79	5.07	6.67	4.27	6.98	5.52	4.44	6.77	2.26	5.79	6.63	10.5	9.87	9.24
Ba	781	728	389	408	527	201	856	566	422	1385	670	497	438	468
Hf	5.68	6.13	4.51	4.36	4.72	1.86	3.86	4.58	2.14	3.55	4.01	3.65	4.08	4.13
Ta	1.2	1.1	1.06	0.82	1.03	0.51	0.93	1.1	0.5	0.82	0.47	1.11	1.15	1.12
Tl	0.63	0.61	0.55	0.42	0.58	0.36	0.45	0.62	0.28	0.60	0.72	0.71	0.67	0.61
Pb	25.3	24.8	17.6	14.7	19.7	13.8	15.5	19.8	14	23.9	23.1	26.1	21.9	24.8
Bi	0.63	0.36	0.27	0.19	0.32	0.18	0.18	0.30	0.14	0.31	0.06	0.48	0.46	0.43
Th	14.8	12.5	10.7	7.61	12.2	6.95	8.68	12.8	5.69	10.8	13.3	14.1	11.5	12.1
U	2.64	2.83	2.83	3.16	3.9	5.58	2.12	2.76	5.03	4.08	2.51	2.83	4.92	4.99
Cr/Ni	1.99	2.02	2.19	1.85	2.03	1.58	2.08	1.99	1.40	1.78	2.31	2.01	2.21	2.22
Ni/Co	1.78	1.44	2.73	2.70	2.18	2.59	2.48	2.08	2.17	2.11	1.81	2.47	2.68	2.63
Sc/Ni	0.43	0.55	0.36	0.35	0.41	0.28	0.34	0.42	0.39	0.44	0.53	0.38	0.35	0.42
Sc/Cr	0.22	0.27	0.16	0.19	0.20	0.18	0.16	0.21	0.28	0.25	0.23	0.19	0.16	0.19
Th/Sc	1.16	0.92	1.09	0.92	1.11	0.88	1.03	1.12	0.80	0.95	0.94	0.95	0.79	0.76
Zr/Sc	14.45	15.74	15.53	16.57	14.55	7.50	14.95	13.95	9.43	9.74	9.57	7.58	8.69	7.55
Cr/Th	3.99	4.02	5.64	5.66	4.46	6.29	5.92	4.26	4.46	4.25	4.58	5.62	7.93	6.88
Co/Th	1.13	1.38	0.94	1.13	1.01	1.54	1.15	1.03	1.47	1.13	1.10	1.13	1.34	1.18

was composed of mainly quartz and feldspars, with some rock clasts. Grain size of the samples ranged between 0.25 and 0.05 mm and 0.05–0.01 mm, and hence was effective for heavy mineral analyses.

The heavy and light minerals in all the Huangdigou sections were predominantly sub-angular to sub-round. The ilmenite, magnetite, limonite, and garnet were the abundant detrital minerals present in the section, together occupying ~36–82% (Fig. 6). All the minerals are unstable and varied through the sections. According to Wang and Li (2003), the assemblage of limonite, barite, tourmaline, rutile, anatase, and zircon are mainly derived from sedimentary rocks, while the assemblage of tourmaline, rutile, anatase, zircon, sphene, apatite, monazite, and amphibole primarily originate from acidic magmatic rocks. Likewise, the assemblage of garnet, epidote, sillimanite, and leucoxene is concentrated in metamorphic rocks. Thus, according to the contents of the heavy minerals (Fig. 6), unit 1 was dominantly composed of sedimentary rocks, with a few acidic magmatic and metamorphic rocks.
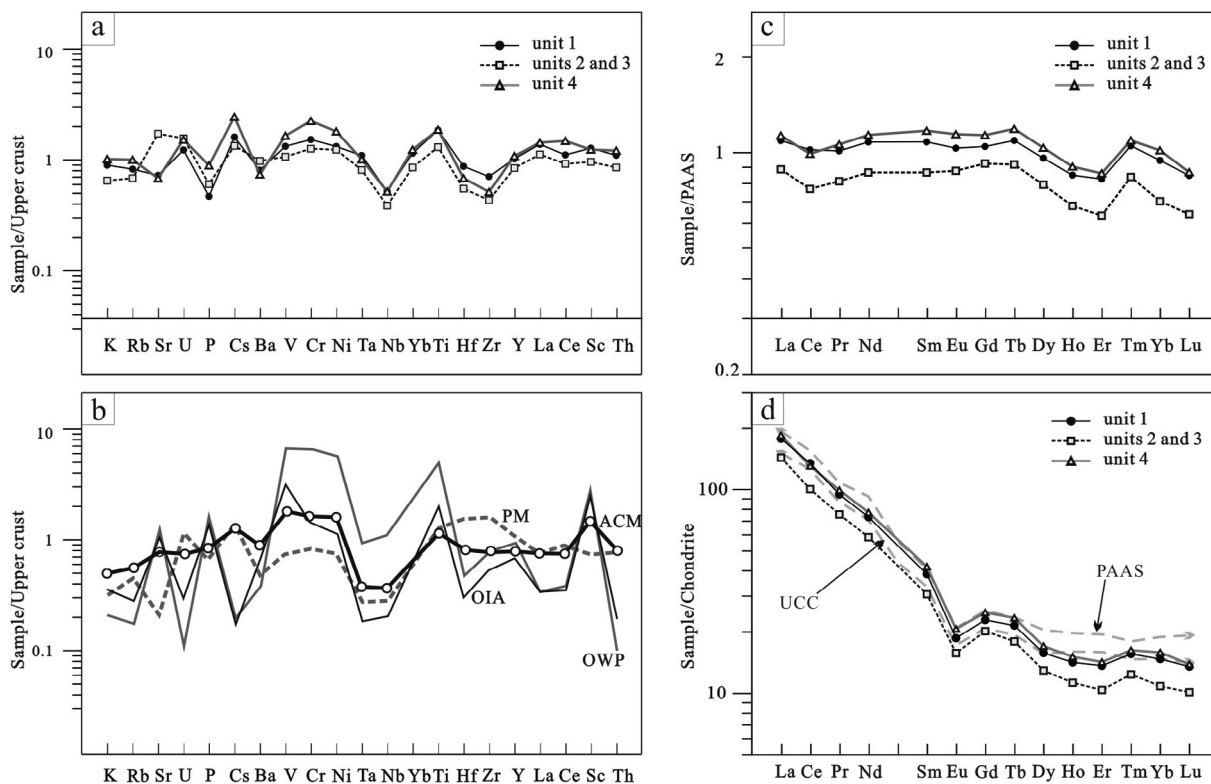
Fig. 8. Spider diagrams and REE patterns of unit averages for the Huangdigou section. (a) Normalized to average upper continental crustal values (after Floyd et al., 1991). (b) Expected values for comparison for passive margin (PM), active continental margin + continental island arc (ACM), oceanic within-plate (OWP), and continental island arc (OIA) settings. (c) REE normalized to PAAS and (d) to chondrite (after Taylor and McLennan, 1985).

Table 5
Rare element concentrations (ppm) for silts and mud of the Huangdigou section.

Unit	Unit 1					Units 2–3				Unit 4				
Sample	Pm 01–6	Pm 09–4	Pm 05–24	Pm 05–22	Pm 05–20	Pm 05–13	Pm 05–9	Pm 02–25	Pm 02–18	Pm 02–16	Pm 02–14	Pm 02–1	Pm 07–9	Pm 07–2
La	51.3	52.8	36.3	28.3	38.7	22.9	35.4	46.4	25.6	38.1	45.9	40.7	39.1	46.4
Ce	109	110	63.8	50	75.8	42.7	61.4	86.8	45.5	71.2	86.1	77.6	71.2	82.3
Pr	10.8	11.5	7.86	6.26	8.64	4.89	7.63	10.1	5.3	8.25	9.98	8.99	8.73	10.1
Nd	40.4	43.8	30.6	24.5	33.6	18.8	29.2	38.7	20	31.9	37.7	34.7	33.8	39.4
Sm	6.49	7.69	5.59	4.5	6.01	3.38	5.18	6.79	3.36	5.55	6.44	6.35	6.38	7.1
Eu	1.18	1.27	1.14	0.96	1.13	0.69	1.07	1.28	0.69	1.1	1.19	1.27	1.16	1.41
Gd	5.19	5.58	4.91	4	4.89	3.21	4.83	5.61	3.04	5.04	5.3	5.39	4.86	5.8
Tb	0.80	0.98	0.85	0.69	0.88	0.52	0.77	0.97	0.47	0.80	0.92	0.93	0.86	0.95
Dy	4.04	4.74	4.6	3.58	4.19	2.47	3.89	4.69	2.43	3.96	4.38	4.72	4.26	4.88
Ho	0.83	1.02	0.89	0.69	0.83	0.49	0.76	0.91	0.45	0.79	0.84	0.92	0.85	1.00
Er	2.43	2.85	2.44	1.95	2.31	1.27	2.06	2.51	1.18	2.16	2.19	2.52	2.44	2.83
Tm	0.42	0.51	0.42	0.36	0.40	0.24	0.38	0.43	0.24	0.40	0.38	0.42	0.45	0.50
Yb	2.65	3.3	2.56	2.23	2.5	1.45	2.16	2.63	1.34	2.26	2.37	2.67	3.02	3.33
Lu	0.39	0.42	0.36	0.29	0.36	0.18	0.31	0.37	0.19	0.33	0.34	0.38	0.37	0.41
ΣREE	235.9	246.5	162.3	128.3	180.2	103.2	155.0	208.2	109.8	171.8	204.0	187.6	177.5	206.4
LREE	219.2	227.1	145.3	114.5	163.9	93.4	139.9	190.1	100.4	156.1	187.3	169.6	160.4	186.7
HREE	16.7	19.4	17.0	13.8	16.4	9.8	15.2	18.1	9.3	15.7	16.7	17.9	17.1	19.7
LREE/HREE	13.09	11.70	8.54	8.31	10.02	9.50	9.23	10.49	10.75	9.92	11.20	9.45	9.37	9.48
Eu/Eu*	0.60	0.57	0.65	0.68	0.62	0.63	0.64	0.62	0.64	0.62	0.60	0.65	0.61	0.65
La/Sc	4.01	3.88	3.69	3.42	3.52	2.91	4.20	4.07	3.62	3.34	3.26	2.73	2.70	2.92
La/Th	3.47	4.22	3.39	3.72	3.17	3.29	4.08	3.63	4.50	3.53	3.45	2.89	3.40	3.83
(La/Sm)cn	5.10	4.43	4.19	4.06	4.16	4.37	4.41	4.41	4.92	4.43	4.60	4.14	3.96	4.22
(La/Yb)cn	13.89	11.48	10.17	9.10	11.10	11.33	11.76	12.66	13.70	12.09	13.89	10.93	9.29	9.99
(Gd/Yb)cn	1.62	1.40	1.59	1.48	1.62	1.83	1.85	1.76	1.88	1.84	1.85	1.67	1.33	1.44

Note: cn, chondrite normalization.

Units 2 and 3 were mainly formed from acidic magmatic rocks, with a few metamorphic rocks, while unit 4 by both metamorphic and acidic magmatic rocks, along with some sedimentary rocks. This also indicates that the main source areas in units 1–3 are single, whereas mixed in unit 4. Fig. 7a is a Q-F-L diagram that clearly shows the low quartzose, high lithic content in unit 1, but sub-equal amounts of quartz and feldspar in units 2–4. The sandstone samples in unit 1 fall within the field of undissected arc setting, while those in units 2–4 fall within the
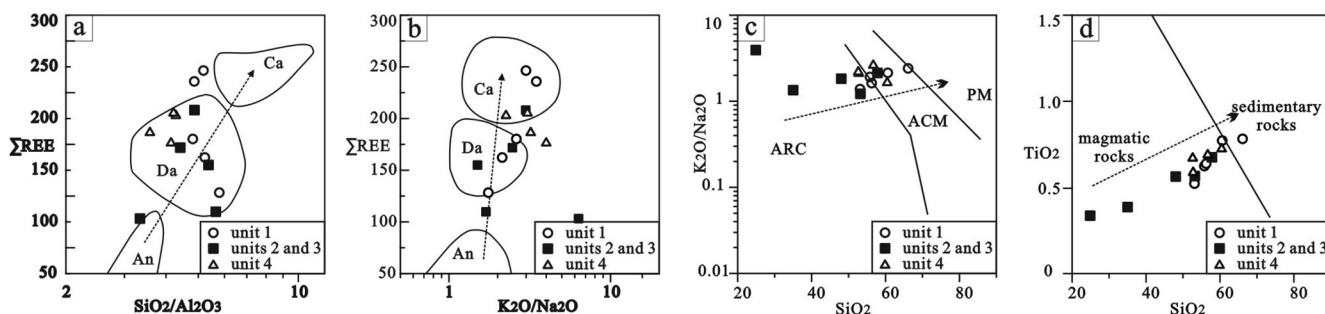
Fig. 9. Discrimination diagrams illustrating provenance rocks of the Huangdigou section sediments. (a) SiO_2-K_2O/Na_2O diagram, (b) SiO_2-Ti_2O diagrams (after Roser and Korsch, 1986), (c) SiO_2/Al_2O_3 vs. ΣREE relationship and (d) K_2O/Na_2O vs. ΣREE relationships (after Bhatia, 1985). Components: An, andesitic source rocks; Da, dacitic source rocks; Ca, Granite-gneiss and sedimentary source rocks.
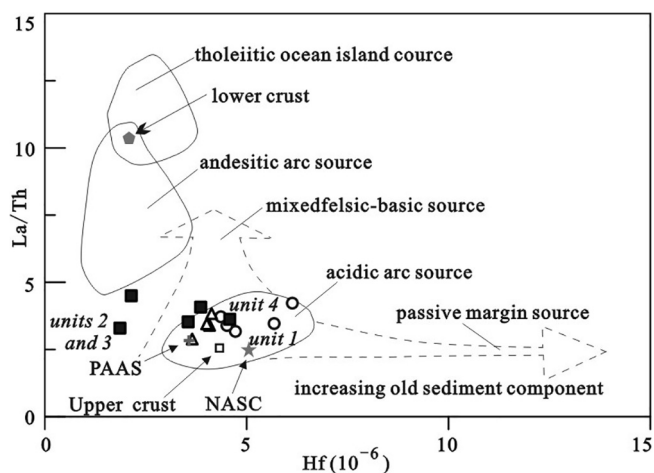

Fig. 10. Discrimination diagrams illustrating sediment recycling and provenance of the Huangdigou section. La/Th vs. Hf diagram (after Floyd and Leveridge, 1987). PAAS and UCC values are from Taylor and McLennan (1985), and the NASC value is from Gromet et al. (1984).

field of dissected arc setting. This indicates that a more acidic arc source component is occupied in unit 1, as opposed to an andesitic arc source component in units 2–4.

4.3. Geochemistry of mud and silts of the Huangdigou section

4.3.1. Major elements

The samples from the Huangdigou section show a general variation in chemical composition, with SiO_2 content ranging from 24 to 66 wt%, Al_2O_3 from 6.2 to 14.71 wt%, K_2O between 1.4 and 3.09 wt%, and Na_2O contents between 0.36 and 1.82 wt% (Table 3). According to the geochemical classification of Pettijohn et al. (1987), there are nine litharenites and five arkoses (Fig. 7b). As per the SiO_2/Al_2O_3 and Fe_2O_3/K_2O classification diagram of Herron (1988), 10 of the analyzed sediments have been classified as unstable immature wackes and only four samples as shale (Fig. 7c).

4.3.2. Trace elements

Table 4 displays the trace element concentrations of the analyzed samples of the Huangdigou section. Compared to the post-Archean Australian Shale (PAAS) (Taylor and McLennan, 1985) values, the concentrations of Cs (4.44–9.87 ppm), Ba (201–856 ppm), Rb (49.3–120 ppm), Sr (129–1293 ppm), and Sc (7.07–15.90 ppm) showed general scatter. However, their mean concentrations are similar to PAAS (Fig. 8c). In general, the samples from units 1 and 4 are characterized by slightly higher concentrations of Zr and Hf, and lower Nb and Ta, as opposed to the samples from units 2 and 3. All the samples showed high correlations of Zr-Hf and Nb-Ta, with R^2 values of 0.97

and 0.79, respectively. The abundance of Co (8.62–17.3 ppm), Ni (18.1–41.2 ppm), V (46.5–113 ppm), Cr (43.1–91.2 ppm), and Sc (8.43–15.9 ppm) were variable, although the ratios of Cr/Ni (1.58–2.31), Ni/Co (1.44–2.70), Sc/Ni (0.28–0.55), and Sc/Cr (0.16–0.28) were concentrated. Samples of unit 1 revealed the highest concentrations of ferromagnesian trace elements, followed by unit 4 samples, and the least by units 2 and 3, implying a more mafic composition in the provenance of the unit 1. The averaged elemental values for the samples from each phase were normalized to average upper continental crust (UCC) (Taylor and McLennan, 1985) reference values (Fig. 8a). Several deviations from UCC values were observed in units 1 and 4, which included negative Sr, P, Ba, Nb, and Zr anomalies, positive U, Cs, and V-Cr-Ni anomalies, and slightly positive Yb-Ti anomalies. Units 2 and 3, however, displayed negative K-Rb, P, Nb, and Zr anomalies, and considerable Sr-U, Cs, and Yb-Ti anomalies.

4.3.3. Rare earth elements

Total REE (ΣREE) abundance in the Huangdigou section showed variability (Table 5), although all samples exhibited light REE (LREE)-enriched chondrite-normalized REE patterns, similar to UCC and PAAS (Fig. 8c and d). Likewise, the samples exhibited LREE enrichment, with high (La/Sm)cn, (La/Yb)cn, and ΣLREE/ΣHREE, relatively flat HREE ((Gd/Yb)cn = 1.33–1.88), and significant negative Eu anomalies (Eu/Eu* = 0.57–0.68). The total REE concentrations of different units were similar, and there were no systematic differences in the REE patterns amongst the different stratigraphic units (Fig. 8c and d). ΣREE/Al ratios ranged from 12.26 to 18.18, which are higher than UCC (9.68; Taylor and McLennan, 1985), suggesting that non-clay detrital phases contribute significantly to the ΣREE content of the clastic sediments in the section (Singh and Rajamani, 2001; López et al., 2005). However, Zr showed moderate correlation with ΣREE, ΣLREE, and ΣHREE (R^2 = 0.545, 0.515, and 0.691, respectively), suggesting the influence of heavy-mineral zircon upon the total REE content, possibly because it is largely controlled by irregular distribution during the sedimentation processes (López et al., 2005).

5. Discussion

5.1. Interpretation of the source areas of the Sanmenxia Basin

5.1.1. Source-rock composition from geochemistry

Multi-element spider diagrams are effective indicators of tectonic environments and source-rock compositions. In reference to the UCC normalized spider diagram proposed by Floyd et al. (1991), samples of units 1 and 4 displayed rather higher values of Cs and V-Cr-Ni, and distinctively lower values of Sr, Nb, and Zr (Fig. 8a). These indicate a minor influence of mature sedimentary detritus in the units (Floyd et al., 1989). However, units 2 and 3, with considerable normal Sr-U, Cs, and Yb-Ti anomalies, showed addition of immature sedimentary detritus as compared to the other two units (Floyd et al., 1989). Upon
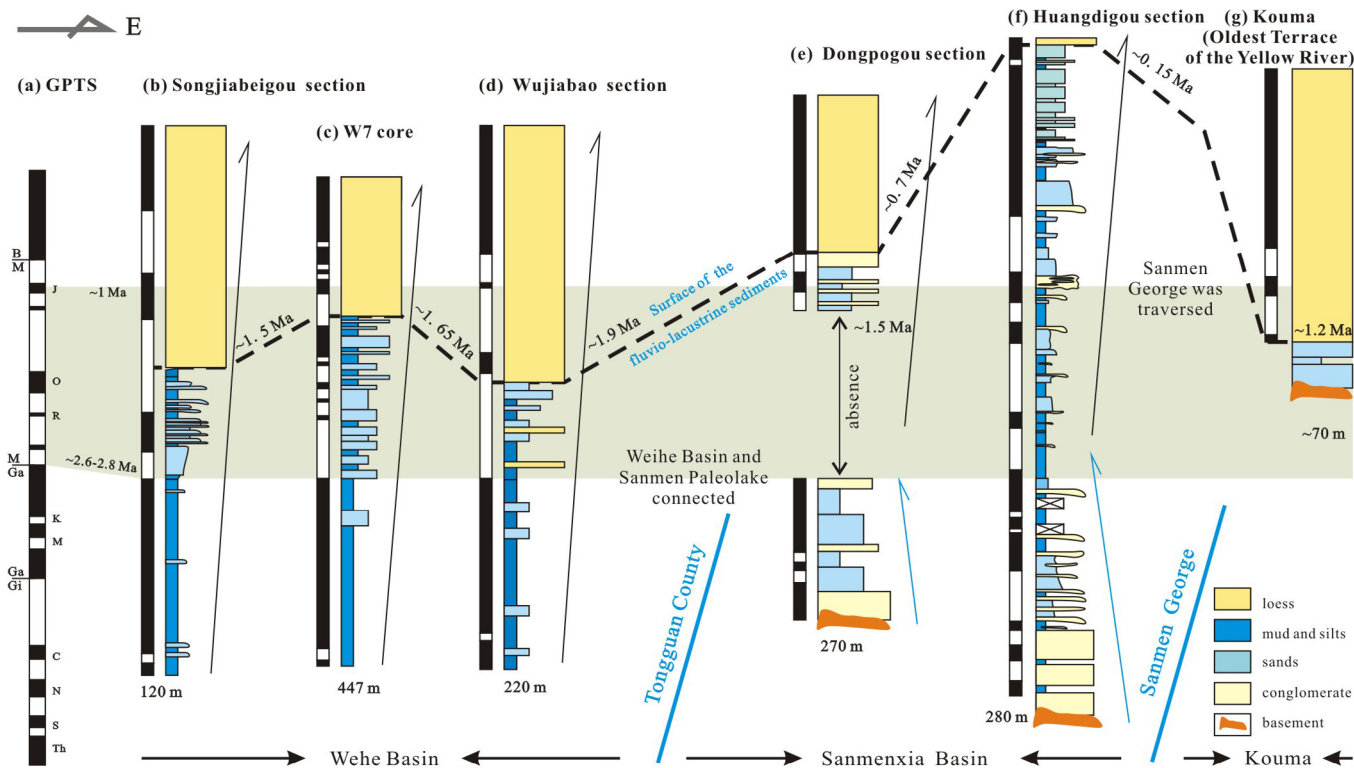
Fig. 11. Stratal correlation of the Sanmen formation and the overlaid Aeolian Loess in the Weihe Basin, the Sanmenxia Basin and the Kouma area. (a) GPTS is from Gradstein et al. (2012). The ages of the W7 borehole (c), Wujiabao section (d) in Weihe Basin, Dongpogou section (e) in Sanmenxia Basin and Oldest terrace of the Yellow River (g) near Kouma are from Ge et al. (1991), Sun et al. (1984), Cao et al. (1985) and Pan et al. (2005a, 2005b), respectively.

comparing the obtained average values of units 1, 2, 3, and 4 to the Passive Margin (PM), Active Continental Margin (ACM), Oceanic Island Arc (OIA), and Oceanic within-plate (OWP) settings (Fig. 8b), the spider-diagram patterns of the three units displayed better association to a continental island arc/an ACM setting, indicating a dacitic to granodioritic source-rock composition.

The REE and Eu composition of sedimentary rocks are the most reliable indicators of provenance (Bhatia, 1985; Taylor and McLennan, 1985; McLennan, 1989). The significant enrichment of LREEs and the flat HREE patterns of the clastics in the Huangdigou section (Table 5 and Fig. 8d) suggest that the source rocks were chiefly felsic, while the distinct negative Eu anomaly signifies a differentiated source, akin to granite or rhyolite. Europium anomalies for all the samples (0.61–0.68, average = 0.65, Table 5) are similar to the average value of 0.65 for croton-derived PAAS (Fig. 8d).

Some elements and their ratios, such as SiO_2/Al_2O_3, K_2O/Na_2O, Th/Sc, La/Sc, Zr/Sc, and Co/Th, are particularly sensitive to the average source composition (Bhatia, 1985; Taylor and McLennan, 1985; Roser and Korsch, 1986; Girty et al., 1996). The SiO_2-K_2O/Na_2O ratio, SiO_2-Ti_2O diagrams (Roser and Korsch, 1986), and the SiO_2/Al_2O_3 and K_2O/Na_2O vs. ΣREE relationships (Bhatia, 1985) suggest that the sediments in units 1 and 4 mainly derived from sedimentary-granodioritic to dacitic source components (active continental margin to continental island arc). On the contrary, the sediments in units 2 and 3 derived primarily from dacitic source components (continental island arc) (Fig. 9). The Th/Sc (0.76–1.16, average = 0.96) and La/Sc ratios (2.70–4.20, average = 3.45) of the section demonstrate properties between continental island arc (0.85 and 1.82, respectively) and active continental margin (2.59 and 4.55, respectively) settings (Bhatia and Crook, 1986). However, Th/Sc and La/Sc ratios for samples in unit 1 (average of 1.03 and 3.70, respectively) are higher than those in units 2, 3 and 4, thereby displaying characteristics of the active continental margin setting, and more felsic components (Bhatia and Crook, 1986). Floyd and Leveridge (1987) established a discrimination diagram using

the La/Th ratio vs. Hf to determine different arc components and sources (Fig. 10). Uniformly high La/Th ratios (3.29–4.20, average = 3.81) and low Hf contents (1.86–4.58 ppm, average = 3.20 ppm) for units 2 and 3 suggest their derivation predominantly from a mixed felsic-acidic source (Gill, 1981). Thus, these results suggest a relatively felsic source rock in the Huangdigou section, but with a dominant mafic source rock in units 2 and 3.

5.1.2. Source areas of the Sanmenxia Basin

The aforementioned geochemical features of the analyzed samples are indicative of mixed, multi-source sediments, including felsic and some mafic rocks for the sediments of the Huangdigou section. Unit 1 is mainly composed of acidic arc source components, units 2 and 3 derived from andesitic arc source components, and unit 4 is composed of acidic-andesitic arc source. Because the ability to resist weathering varies across different rocks, different rock assemblages can be preserved in varied grains. Thus, the heavy mineral analyses revealed sedimentary components, acidic magmatic rocks, and both acidic magmatic and metamorphic components preserved in unit 1, units 2 and 3, and unit 4 of the Huangdigou section, respectively (Fig. 6). At the same time, the coarse clasts composition (Fig. 3) implies the intermediate-basic magmatic and intermediate-acidic magmatic components in the section. From the analyses of the paleocurrents (Fig. 3) and the geological map (Fig. 1b), we infer that the main source areas of the Sanmenxia Basin changed from Zhongtiao Mountain in unit 1 (sedimentary rocks, with minor metamorphic rocks) to western part of the Qinling Orogen in units 2 and 3 (acidic magmatic rocks with minor metamorphic and sedimentary rocks), and then to both the former two areas in unit 4 (metamorphic rocks in Zhongtiao Mountain and acidic magmatic rocks in North Qinling). Moreover, the different Zircon U-Pb age distributions between unit 1 (SM19) and unit 2 (SM21 and SM22) of the Songjiabeigou section (Kong et al., 2014) indicate the different source areas in the Weihe Basin.
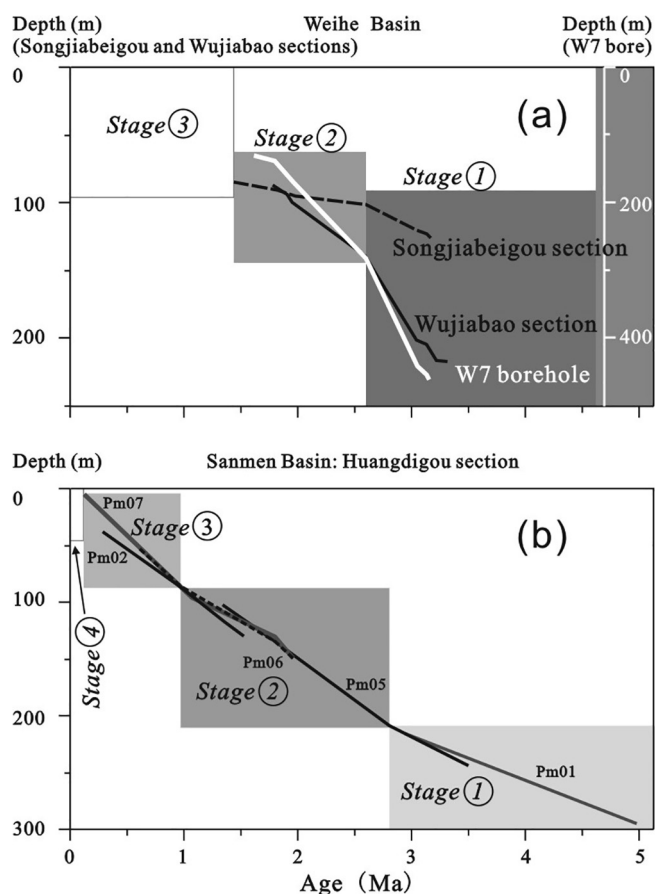
Fig. 12. Thickness and ages of the Pliocene-Pleistocene sections and drill in the Weihe Basin and the Sanmenxia Basin, showing the varied sedimentary rates of the sections or borehole in Fig. 11.

5.2. Tectonically controlled evolution of the paleo-Yellow River

Based on our research and previous studies on the sections in the Weihe Basin (Sun et al., 1984; Ge et al., 1991; Hu et al., 1993), Sanmenxia Basin (Cao et al., 1985; Wang et al., 1999), and Kouma area (eastern part of the Sanmenxia Basin; Pan et al., 2005a), a cross section from west to east could be established (Fig. 11). From this cross section, it could be observed that the sedimentary environments varied from the Weihe Basin to the Sanmenxia Basin. The Songjiabeigou section, W7 borehole, and Wujiabao section shows that the Weihe Basin shifted from deeper water environments in Pliocene to shallower water environments in early Pleistocene. The Sanmenxia Basin, however, experienced diametrically opposite evolutionary history, with a deepening-upward water environment during the same era in both the Dongpogou and Huangdigou sections.

This is consistent with the sedimentary rates of the sections (Fig. 12) and the change in the source areas of the basins. These differences are also consistent with the regional stress regime proposed by Shi et al. (2015), i.e., a transtensional stress regime of NW–SE extension and NE–SW compression in the late Miocene–early Pleistocene, which changed to a less intense NE–SW extension in the early-late Pleistocene. We suggest that the Sanmenxia and Weihe basins interconnected at ~2.6–2.8 Ma, and the Yellow River traversed the Sanmen George at ~1.0 Ma, as described in detail in Section 5.2.1.

5.2.1. Prior to the traversing of the Yellow River in the Pliocene

During the Pliocene, influenced by the NW-SE extensional stress regime (Shi et al., 2015), and the rapid uplift of the western part of the Qinling Orogen (Hua and Taibai mountains) and the Zhongtiao

Mountain (Liu, 2009; Liu et al., 2013) from late Miocene, the pre-existing northeast-striking and northwest-dipping normal faults were reactivated (F1 and F2 in Fig. 13a–c). The alluvial fan in the Sanmenxia Basin and the shallow lake in the Weihe Basin can be explained by both being intermontane basins that were separate from each other (Fig. 13a). Consequently, we interpret that there existed a joint Zhongtiao-Hua mountain range in the Pliocene, which prevented the connection of the two basins.

5.2.2. Connection of the Sanmenxia and Weihe basins at ~2.8–2.6 Ma

The subsequent and weaker northeast-southwest extensional regime from the early Pleistocene (Shi et al., 2015) played an important role in separating the Hua and Zhongtiao mountains, as the northwest-striking faults were activated (F3 and F4 in Fig. 13b), accompanied by a strike-slip movement at F1 and F2. The sedimentation results of this study, combined with pollen data from Tong et al. (2000) and ostracod data from Wang et al. (2010) indicate that a drier environment succeeded the wetter Pliocene environment in the Weihe Basin at ~2.6 Ma. In contrast, the sedimentation results and ostracod assemblages (Yuan, 1986) imply a lake expansion in the Sanmenxia Basin at the same time (~2.8 Ma). Moreover, the sedimentation rates of the two basins during the same period were also different (Fig. 12). For the Sanmenxia Basin, the sedimentation rate was lower during the Pliocene than in the early Pleistocene, whereas in case of the Weihe Basin, it was much higher in the Pliocene than in the early Pleistocene. Such differences indicate that it was tectonic control, rather than the influence of regional climate, which was probably responsible for the coarsening-upward succession of the Weihe Basin and the coeval fining-upward trend of the Sanmenxia Basin strata. Moreover, the acidic magmatic clasts derived from the Hua and Taibai mountains, which are rare in the Zhongtiao Mountain (Fig. 1), were deposited in abundance in the Sanmenxia Basin from ~2.8 Ma onwards. Together, all these results suggest that the Sanmenxia and Weihe basins became connected after ~2.8–2.6 Ma, as the paleo-Yellow River incised the Tongguan County area (Fig. 13b). Channel avulsion processes between these two basins led to the rapid draining of the Weihe Basin, and conversely, rapid flooding of the Sanmenxia Basin, thus depositing different succession trends in the two basins. Because of this traversing, the water level difference (Fig. 13a) between the two basins was eliminated (Fig. 13b).

5.2.3. Traversing of the Sanmen Gorge at ~1.0 Ma

At ~1.0 Ma, the continued NE–SW extensional regime from the early Pleistocene (Shi et al., 2015) sustained the strike-slip of F2 and extension of F4. Consequently, the sedimentary environment and provenance in the Sanmenxia Basin changed again. After ~1.0 Ma, the fluvial facies with few ostracods (Yuan, 1986) replaced the shallow lake and lakeshore environment of ~2.6–1.0 Ma, implying that the basin experienced rapid drying up. Additionally, the provenance of the Sanmenxia Basin shed from both the western part of the North Qinling (Hua and Taibai mountains) and the Zhongtiao Mountain. In the Weihe Basin, the fluvio-lacustrine sediments were gradually replaced by eolian loess after ~1.9–1.5 Ma near the basin margin (Figs. 11a–c and 13c). These findings suggest new uplift of the nearby mountains, which lowered the base level of the Yellow River and provided the precondition for the final traversing of the Sanmen Gorge, or make the faults to remain active. Thus, the clasts from the western part of the Qinling Orogen observed in the Sanmenxia and Weihe basins in the earlier stage might have been transported to lower levels along the outflow from the Sanmen Gorge after ~1.0 Ma. This timing of traverse is also supported by the appearance of the oldest terraces near the Sanmen Gorge and Kouma at ~0.9–1.2 Ma (Pan et al., 2005a, 2005b; Su et al., 2009).

5.3. Factors that triggered the evolution of the Yellow River

As discussed above, the initial deposition of the Sanmen Formation
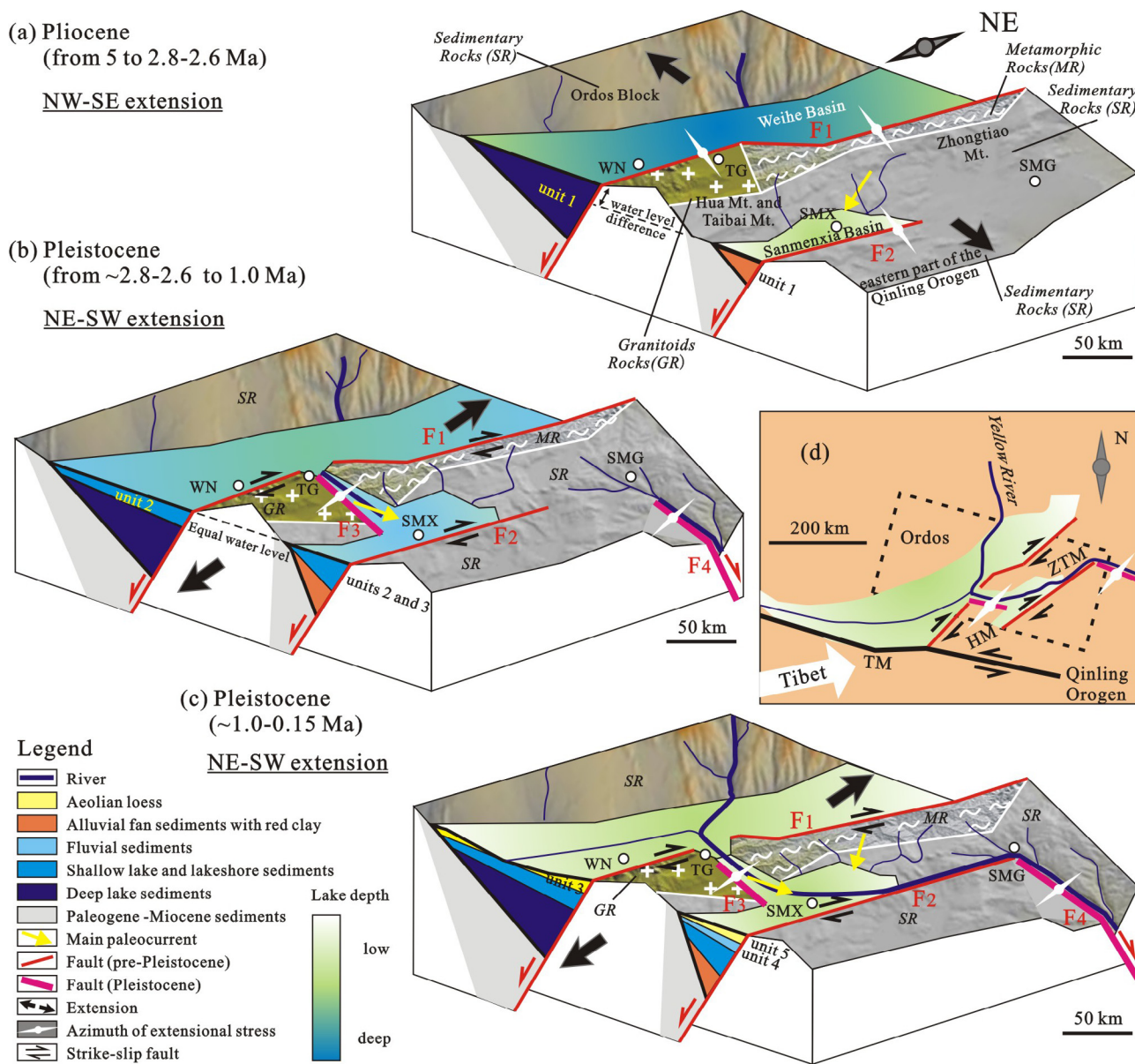
Fig. 13. (a), (b) and (c) Schematic map showing model of the Sanmenxia Basin, the Weihe Basin and the paleo-Yellow River evolution in Pliocene to Pleistocene, which was controlled by the regional regime shift (Shi et al., 2015). (d), Regional regime state of the third stage (c). Abbreviations: WN-Weinan City; SMX-Sanmenxia City; TG-Tongguan; SG-Sanmen George; HM-Hua Mountain; ZTM-Zhongtiao Mountain.

in the Sanmenxia Basin, the connection of the Sanmenxia and Weihe basins, and the traversing of the Sanmen Gorge were coeval with the transition in the regional regime (Shi et al., 2015). This suggests that tectonic evolution was the major factor that triggered the evolution of the basins and the paleo-Yellow River.

The initial deposition in the basins during the early Pliocene (from ~5 Ma, or earlier) and the timing of the traversing at ~2.8–2.6 Ma and ~1.0 Ma are consistent with many geological events around the Ordos Block, which are related to the rapid uplift of the Tibetan Plateau. In the Weihe Basin, for example, the Hua, Taibai, and Zhongtiao mountains experienced rapid uplift from the late Miocene (Enkelmann et al., 2006; Liu, 2009; Liu et al., 2013). The basal ages of the Weihe River terraces are ~2.60, 1.20, 0.90, 0.65, and 0.15 Ma (Sun, 2005)., while in the Fen-wei Graben, terraces around the Zhongtiao Mountain developed from ~1.2 Ma (Hu et al., 2012). The red clay that initially formed at ~8.1 Ma in the Liupan Mountain chronicles tectono-geomorphologic events of the northeastern Tibetan Plateau at ~8.1, 2.6–2.5, and 1.7–1.6 Ma (Shi et al., 1999; Song et al., 2007). In the Hejiakouzi

section of the southern Ningxia province, lake deposits ceased to form at ~2.3–1.9 Ma (Shen et al., 2001). In addition, the Helan Mountain on the western margin of the Ordos Block experienced rapid uplift from the late Miocene (Liu et al., 2010). In the Shanxi Graben, sedimentary environment and source area of the Nihewan Basin changed during the late Miocene to Pleistocene at ~10–8 Ma, ~2.8–2.6 Ma, and 1.8 Ma (Chen et al., 2012, 2015; Liu et al., 2018). Transitions from alluvial fan/red clay to delta and lacustrine at ~2.6 Ma, and then to fluvial or eolian loess at ~1.0–1.2 Ma was recorded in the Linfen Basin (Li et al., 2004; Chen et al., 2016). Furthermore, some segments of the Yellow River were formed at ~1.0 Ma. For example, the multi-wave headward erosion of the Jinshan Gorge at ~1.2 Ma to 11 ka (Pan et al., 2012; Hu et al., 2016), the strata terraces along the Yellow River extending back to ~1.24 Ma near Lanzhou (Pan et al., 2009), and the current drainage system of the Yellow River around Hetao Basin, was completely established by at least ~1.2 Ma (Li et al., 2017). Therefore, the rapid uplift of the Tibetan Plateau from the late Miocene (Molnar and Tapponnier, 1975; Peltzer et al., 1985; Yin and Harrison, 2000;

Tapponnier et al., 2001; Liu et al., 2004; Yin, 2010) could have been the main trigger of the evolution of the paleo-Yellow River in the Weihe region. This possibly led to the out-of-phase evolution of the Sanmenxia and Weihe basins, which subsequently became linked because of the evolution of the strike-slip faults (Figs. 1b and 13d).

Sedimentation and provenance analysis of the half-graben basins clearly reflect the pattern and timing of the tectonic processes. Moreover, sedimentary facies and provenance studies could become the best records of tectonic events in the extensional tectonic setting, upon the addition of age constraints using paleontology and magnetostratigraphy.

6. Conclusions

(1) The Pliocene-Pleistocene Huangdigou section in the Sanmenxia Basin was deposited in a series of five types of environment: alluvial fan between ~5 Ma to ~2.8 Ma, shallow lake between ~2.8–1.8 Ma, lakeshore between ~1.8–1.0 Ma, fluvial between ~1.0–0.15 Ma, and eolian loess after ~0.15 Ma.

(2) The Songjiabeigou section contains deposits representing three sedimentary facies: deep lake prior to ~2.6 Ma, shallow lake between ~2.6 Ma and ~1.5 Ma, and eolian loess after ~1.5 Ma.

(3) The main source rocks of the Sanmenxia Basin, as revealed by heavy mineral and geochemical analyses, are sedimentary rocks from Zhongtiao Mountain at ~5–2.8 Ma, acidic magmatic rocks from western part of the Qinling Orogen at ~2.8–1.0 Ma, and both acidic magmatic and metamorphic rocks from the two areas at ~1.0–0.15 Ma.

(4) The Sanmenxia and Weihe basins became interconnected with each other at ~2.8–2.6 Ma, and the Yellow River traversed the Sanmen Gorge at ~1.0 Ma. The main factor controlling the drainage and basin evolution may have been the variable regional tectonic regime in the Weihe Graben during the late Miocene.

Declaration of Competing Interest

None.

Acknowledgements

References

Allen, J.R.L., 1970. Studies in fluviatile sedimentation: a comparison of fining-upwards cyclothems, with special reference to coarse-member composition and interpretation. J. Sediment. Petrol. 40 (1), 298–323.
An, Z., Kutzbach, J.E., Prell, W.L., Porter, S.C., 2001. Evolution of Asian monsoons and phased uplift of the Himalaya-Tibetan plateau since Late Miocene times. Nature 411 (6833), 62–66.
Bhatia, M.R., 1985. Rare earth element geochemistry of Australian Paleozoic graywackes and mudrocks: provenance and tectonic control. Sed. Geol. 45 (1), 97–113.
Bhatia, M.R., Crook, K.A., 1986. Trace element characteristics of graywackes and tectonic setting discrimination of sedimentary basins. Contrib. Miner. Petrol. 92 (2), 181–193.
Cant, D.J., Walker, R.G., 1976. Development of a braided-fluvial facies model for the Devonian Battery Point Sandstone, Quebec. Can. J. Earth Sci. 13 (1), 102–119.
Cao, Z., Xing, L., Xu, Q., 1985. A preliminary study of the magnetic stratigraphy of the dongpogou section in the sanmen gorge area. Bull. Inst. Geomech. CAGS 5, 65–74 (in Chinese with English abstract).
Chen, X., Shi, W., Hu, J., Dong, S., 2016. Sedimentation of the pliocene-pleistocene chaizhuang section in the central of linfen basin, north china and its tectonic significance. J. Geomech. 22 (4), 984–993 (in Chinese with English abstract).
Chen, X., Chi, Z., Yan, Z., Wang, Y., Min, L., Yao, P., Dong, J., Yao, D., 2012. Features of sedimentary facies of the Nihewan Basin in North China: An example from the

Eastern Taiergou Section. Earth Sci. Front. 19 (4), 227–238 (in Chinese with English abstract).
Chen, X., Chi, Z., Dong, S., Yan, Z., Yang, J., Shi, W., Min, L., Wang, Y., Yao, P., 2015. Late Cenozoic sedimentation of Nihewan Basin, central North China and its tectonic significance. J. Asian Earth Sci. 114, 242–257.
Clark, M.K., Schoenbohm, L.M., Royden, L.H., Whipple, K.X., Burchfiel, B.C., Zhang, X., Tang, W., Wang, E., Chen, L., 2004. Surface uplift, tectonics, and erosion of eastern Tibet from large-scale drainage patterns. Tectonics 23 (1), TC1006.
Clift, P.D., Blusztajn, J., Nguyen, A.D., 2006. Large-scale drainage capture and surface uplift in eastern Tibet–SW China before 24 Ma inferred from sediments of the Hanoi Basin, Vietnam. Geophys. Res. Lett. 33 (19), 1–4.
Craddock, W.H., Kirby, E., Harkins, N.W., Zhang, H., Shi, X., Liu, J., 2010. Rapid fluvial incision along the Yellow River during headward basin integration. Nat. Geosci. 3 (3), 209–213.
Dai, Y., 1983. History of the Yellow River formation and evolution. People's Yellow River 06, 2–7 (in Chinese).
Dickinson, W.R., 1983. Provenance of North American Phanerozoic sandstones in relation to tectonic settings. Geol. Soc. Am. Bull. 94 (2), 222–235.
Enkelmann, E., Ratschbacher, L., Jonckheere, R., Nestler, R., Fleischer, M., Gloaguen, R., Hacker, B.R., Zhang, Y.Q., Ma, Y.S., 2006. Cenozoic exhumation and deformation of northeastern Tibet and the Qinling: Is Tibetan lower crustal flow diverging around the Sichuan Basin? Geol. Soc. Am. Bull. 118 (5–6), 651–671.
Floyd, P.A., Leveridge, B.E., 1987. Tectonic environment of the Devonian Gramscatho basin, south Cornwall: framework mode and geochemical evidence from turbiditic sandstones. J. Geol. Soc. 144 (4), 531–542.
Floyd, P.A., Shail, R., Leveridge, B.E., Franke, W., 1991. Geochemistry and provenance of Rhenohercynian synorogenic sandstones: implications for tectonic environment discrimination. Geol. Soc., London, Spec. Publ. 57 (1), 173–188.
Floyd, P.A., Winchester, J.A., Park, R.G., 1989. Geochemistry and tectonic setting of Lewisian clastic metasediments from the Early Proterozoic Loch Maree Group of Gairloch. Precambrian Res. 45 (1), 203–214.
Ge, T., Fan, L., Xu, X., Li, S., Zheng, H., 1991. Magnetostratigraphic study for borehole W7 from Yancun, Weinan. Mar. Geol. Quat. Geol. 11, 59–71 (in Chinese with English abstract).
Gill, J.B., 1981. Geophysical setting of volcanism at convergent plate boundaries. In: Orogenic Andesites and Plate Tectonics. Springer-Verlag, Berlin, pp. 44–63.
Girty, G.H., Ridge, D.L., Knaack, C., Johnson, D., Al-Riyami, R.K., 1996. Provenance and depositional setting of Paleozoic chert and argillite, Sierra Nevada, California. J. Sediment. Res. 66 (1), 107–118.
Gradstein, F.M., Ogg, J.G., Schmitz, M., Ogg, G., 2012. The Geologic Time Scale. 2 Elsevier, Amsterdam.
Gromet, L.P., Haskin, L.A., Korotev, R.L., Dymek, R.F., 1984. The "North American shale composite": its compilation, major and trace element characteristics. Geochim. Cosmochim Acta 48 (12), 2469–2482.
Hamidullah, S., Jan, M.Q., Khan, M.A., Khattak, M.U.K., 2001. Crustal reworking at Nanga Parbat, Pakistan: Metamorphic consequences of thermal-mechanical coupling facilitated by erosion. Tectonics 20 (5), 712–728.
Herron, M.M., 1988. Geochemical classification of terrigenous sands and shales from core or log data. J. Sediment. Res. 58 (5), 820–829.
Hu, W., Yue, L., Tian, X., 1993. On the magnetostratigraphy of the Songjia-Beigou section, Youhe, Weinan. Geol. Shanxi 2, 26–32 (in Chinese with English abstract).
Hu, W., 1994. The multiple division and comparision of quaternary period strata in Weinan region. Geol. Shaanxi 12 (2), 46–55 (in Chinese with English abstract).
Hu, X., Zhou, T., Cai, S., 2017. The episodic geomorphological-sedimentary evolution of different basins in the Fenwei Graben and its tectonic implication. J. Geog. Sci. 27 (11), 1359–1375.
Hu, Z., Pan, B., Guo, L., Vandenberghe, J., Liu, X., Wang, J., Fan, Y., Mao, J., Gao, H., Hu, X., 2016. Rapid fluvial incision and headward erosion by the Yellow River along the Jinshaan gorge during the past 1.2 Ma as a result of tectonic extension. Quat. Sci. Rev. 133, 1–14.
Hu, Z., Pan, B., Wang, J., Cao, B., Gao, H., 2012. Fluvial terrace formation in the eastern Fenwei Basin, China, during the past 1.2Ma as a combined archive of tectonics and climate change. J. Asian Earth Sci. 60, 235–245.
Jiang, F., Fu, J., Wang, S., Sun, D., Zhao, Z., 2007. Formation of the Yellow River, inferred from loess-palaeosol sequence in Mangshan and lacustrine sediments in Sanmen Gorge, China. Quaternary Int. 175 (1), 62–70.
Kong, P., Jia, J., Zheng, Y., 2014. Time constraints for the Yellow River traversing the Sanmen Gorge. Geochem. Geophys. Geosyst. 15 (2), 395–407.
Li, B., Sun, D., Xu, W., Wang, F., Liang, B., Ma, Z., Wang, X., Li, Z., Chen, F., 2017. Paleomagnetic chronology and paleoenvironmental records from drill cores from the Hetao Basin and their implications for the formation of the Hobq Desert and the Yellow River. Quat. Sci. Rev. 156, 69–89.
Li, Y., Shi, X., Fu, J., Yang, J., 2004. Geomorphic Transformational Event Around 1.2 Ma BP in the Southern Shanxi Province. Scientia Geographica Sinica 24 (3), 297–303 (in Chinese with English abstract).
Liu, J., 2009. Apatite Fission Track (AFT) analysis of the cenozoic extensional exhumation and uplift of the Helan Shan and the Qinling Mountains, and frictional heating along active faults. Insititute of Geology, China Earthquick Administration, pp. 1–93 (in Chinese with English abstract).
Liu, J., Chen, X., Chi, Z., Wang, Y., Min, L., Li, T., 2018. Tectonically-controlled evolution of the late cenozoic Nihewan Basin, North China Craton: Constraints from stratigraphy, mineralogy, and geochemistry. Acta Geologica Sinica-Engl. Ed. 92 (2), 769–785.
Liu, J., Zhang, P., Lease, R.O., Zheng, D., Wan, J., Wang, W., Zhang, H., 2013. Eocene onset and late Miocene acceleration of Cenozoic intracontinental extension in the North Qinling range-Weihe graben: Insights from apatite fission track

thermochronology. Tectonophysics 584, 281–296.

Liu, J., Zhang, P., Zheng, D., Wan, J., Wang, W., Du, P., Lei, Q., 2010. Pattern and timing of late Cenozoic rapid exhumation and uplift of the Helan Mountain, China. Sci. China Earth Sci. 53 (3), 345–355.

Liu, M., Cui, X., Liu, F., 2004. Cenozoic rifting and volcanism in eastern China: a mantle dynamic link to the Indo-Asian collision? Tectonophysics 393 (1–4), 29–42.

Li, Z., Dong, S., Qu, H., 2014. Timing of the initiation of the Jurassic Yanshan movement on the North China Craton: evidence from sedimentary cycles, heavy minerals, geochemistry, and zircon U-Pb geochronology. Int. Geol. Rev. 56, 288–312.

López, J.M.G., Bauluz, B., Fernández-Nieto, C., Oliete, A.Y., 2005. Factors controlling the trace-element distribution in fine-grained rocks: the Albian kaolinite-rich deposits of the Oliete Basin (NE Spain). Chem. Geol. 214 (1), 1–19.

McLennan, S.M., 1989. Rare earth elements in sedimentary rocks; influence of provenance and sedimentary processes. Rev. Mineral. Geochem. 21 (1), 169–200.

Miall, A.D., 1984. Variations in fluvial style in the lower Cenozoic synorogenic sediments of the Canadian Arctic Islands. Sed. Geol. 38 (1–4), 499–523.

Miall, A.D., 1985. Architectural-element analysis: A new method of facies analysis applied to fluvial deposits. Earth Sci. Rev. 22 (4), 261–308.

Miall, A.D., Gibling, M.R., 1978. The Siluro-Devonian clastic wedge of Somerset Island, Arctic Canada, and some regional paleogeographic implications. Sed. Geol. 21 (2), 85–127.

Molnar, P., Tapponnier, P., 1975. Cenozoic tectonics of Asia: Effects of a continental collision. Science 189, 419–426.

Pan, B., Hu, Z., Wang, J., Vandenberghe, J., Hu, X., Wen, Y., Li, Q., Cao, B., 2012. The approximate age of the planation surface and the incision of the Yellow River. Palaeogeogr. Palaeoclimatol. Palaeoecol. 356–357, 54–61.

Pan, B., Su, H., Hu, Z., Hu, X., Gao, H., Li, J., Kirby, E., 2009. Evaluating the role of climate and tectonics during non-steady incision of the Yellow River: evidence from a 1.24Ma terrace record near Lanzhou, China. Quaternary Sci. Rev. 28 (27–28), 3281–3290.

Pan, B., Wang, J., Gao, H., Chen, Y., Li, J., Liu, X., 2005a. Terrace dating as an archive of the run-through of the Sanmen Gorges. Prog. Nat. Sci. 15 (12), 1096–1103.

Pan, B., Wang, J., Gao, H., Guan, Q., Wang, Y., Su, H., Li, B., Li, J., 2005b. Paleomagnetic dating of the topmost terrace in Kouma, Henan and its indication to the Yellow River's running through Sanmen Gorges. Chin. Sci. Bull. 50 (7), 657–664.

Peltzer, G., Tapponnier, P., Zhang, Z., Xu, Z.Q., 1985. Neogene and Quaternary faulting in and along the Qinling Shan. Nature 317 (6037), 500–505.

Peng, W., Nie, J., Wang, Z., Qiang, X., Garzanti, E., Pfaff, K., Song, Y., Stevens, T., 2018. A major change in precipitation gradient on the Chinese Loess Plateau at the Pliocene-Quaternary boundary. J. Asian Earth Sci. 155, 134–138.

Pettijohn, F.J., Potter, P.E., Siever, R., 1987. Sand and Sandstone, second ed. Springer-Verlag, Berlin, pp. 1–553.

Roser, B.P., Korsch, R.J., 1986. Determination of tectonic setting of sandstone-mudstone suites using content and ratio. J. Geol. 635–650.

SBGMR, 1989a. Shanxi Bureau of Geology (SBGMR), Regional Geology of Shanxi Province. Geological Publishing House, Beijing, pp. 1–698 (in Chinese).

SBGMR, 1989b. Shaanxi Bureau of Geology (SBGMR), Regional Geology of Shaanxi Province. Geological Publishing House, Beijing, pp. 1–637 (in Chinese).

Scholle, P.A., Spearing, D., 1982. Sandstone Depositional Environments. The American Association of Petroleum Geologists, Tulsa, Oklahoma, pp. 1–409.

Shen, X., Tian, Q., Ding, G., Wei, K., Chen, Z., Chai, C., 2001. Late cenozoic stratigraphic sequence and its implication to tectonic evolution, Hejiakouzi Area, Ningxia Hui autonomous region. Earthquake Res. China (Engl. Ed.) 15 (4), 156–166.

Shi, W., Cen, M., Chen, L., Wang, Y., Chen, X., Li, J., Chen, P., 2015. Evolution of the late Cenozoic tectonic stress regime in the Shanxi Rift, central North China Plate inferred from new fault kinematic analysis. J. Asian Earth Sci. 114, 54–72.

Shi, Y., Li, J., Li, B., 1999. Uplift of the Qinghai-Xizang (Tibetan) plateau and east Asia environmental change during late Cenozoic. Acta Geogr. Sinica 54, 20–28 (in Chinese with English abstract).

Singh, P., Rajamani, V., 2001. REE geochemistry of recent clastic sediments from the Kaveri floodplains, southern India: implication to source area weathering and sedimentary processes. Geochim. Cosmochim. Acta 65 (18), 3093–3108.

Song, Y., Fang, X., Torii, M., Ishikawa, N., Li, J., An, Z., 2007. Late Neogene rock magnetic record of climatic variation from Chinese eolian sediments related to uplift of the Tibetan Plateau. J. Asian Earth Sci. 30 (2), 324–332.

Su, H., Wang, J., Pan, B., Ming, Q., Li, Q., 2009. Sequences and genesis of the Yellow River terraces from Sanmen Gorge to Kouma. J. Geog. Sci. 19 (3), 351–358.

Sun, J., 2005. Long-term fluvial archives in the Fen Wei Graben, central China, and their bearing on the tectonic history of the India? Asia collision system during the Quaternary. Quat. Sci. Rev. 24 (10–11), 1279–1286.

Sun, J., Zhao, J., Wei, M., Ge, T., Wen, S., Fan, L., Geng, H., 1984. New data of the Wujiabao section. Quaternary Sci. 4, 44–49 (in Chinese with English abstract).

Tapponnier, P., Peltzer, G., Armijo, R., 1986. On the mechanics of the collision between India and Asia. Geol. Soc., London, Spec. Publ. 19 (1), 113–157.

Tapponnier, P., Peltzer, G., Le Dain, A.Y., Armijo, R., Cobbold, P., 1982. Propagating extrusion tectonics in Asia: New insights from simple experiments with plasticine. Geology 611–616.

Tapponnier, P., Xu, Z.Q., Francoise, R., Meyerm, B., Nicolas, A., Gerard, W., Yang, J.S., 2001. Oblique stepwise rise and growth of the Tibet Plateau. Science 294, 1671–1677.

Taylor, S.R., McLennan, S.M., 1985. The Continental Crust: Its Composition and Evolution. Blackwell Scientific Publications, Oxford, U.K., pp. 1–312.

Tong, G., Wu, X., Chen, Y., 2000. Palynoevents since Late Cenozoic in Weihe Valley and Climate Changes. J. Geomech. 6 (4), 18–65 (in Chinese with English abstract).

Wang, B., Zheng, H., Wang, P., He, Z., 2013. The cenozoic strata and depositional evolution of Weihe Basin: Progresses and problems. Adv. Earth Sci. 28 (10), 1126–1135 (in Chinese with English abstract).

Wang, B., Zheng, H., He, Z., Wang, P., Kaakinen, A., Zhou, X., 2014. Middle Miocene eolian sediments on the southern Chinese Loess Plateau dated by magnetostratigraphy. Palaeogeogr., Palaeoclimatol., Palaeoecol. 411, 257–266.

Wang, C., Li, X., 2003. Sedimentary Basin: From Principles to Analyses. China Higher Education Press, Beijing, pp. 1–378 (in Chinese).

Wang, S., Jiang, F., Wu, X., 1999. A study on the age of Sanmen group in Sanmenxia area. J. Geomech. 5 (4), 65–71 (in Chinese with English abstract).

Wang, X., Chen, X., 2005. Stratigraphic division and correlation of each geologic period in China. Geological Publishing House, Beijing, pp. 1–596 (in Chinese with English abstract).

Wang, Z., Wang, P., Wang, X., 2010. Study on the Neogene-Quaternary ostracoda fossils of Sanmen Formation in Songjiabeigou, Weinan, Shaanxi. J. Xi'an Shiyou Univ. (Nat. Sci. Ed.) 1, 35–40 (in Chinese with English abstract).

Yin, A., 2010. Cenozoic tectonic evolution of Asia: A preliminary synthesis. Tectonophysics 488 (1–4), 293–325.

Yin, A., Harrison, T.M., 2000. Geologic evolution of the Himalayan-Tibetan Orogen. Annu. Rev. Earth Planet. Sci. 28, 211–280.

Yuan, F., 1986. Discovery of Ostracods from the san men series and its significance. Acta Micropalaeontologica Sinica 2, 005 (in Chinese with English abstract).

Yue, L., Xue, X., 1996. Paleomagnetism of Chinese Loess. Geological Publishing House, Beijing, pp. 27–70 (in Chinese).

Zhang, J., Yin, A., Liu, W., Ding, L., Xu, X., 2016. First geomorphological and sedimentological evidence for the combined tectonic and climate control on Quaternary Yarlung river diversion in the eastern Himalaya. Lithosphere 8 (3), 293–316.

Zhang, K., 1987. How did the middle reach of the Yellow River formed. The Earth 02, 28–29 (in Chinese).

Zhang, Y., Mercier, J.L., Vergély, P., 1998. Extension in the graben systems around the Ordos (China), and its contribution to the extrusion tectonics of south China with respect to Gobi-Mongolia. Tectonophysics 285 (1–2), 41–75.

Zhang, Y., Ma, Y., Yang, N., Shi, W., Dong, S., 2003. Cenozoic extensional stress evolution in North China. J. Geodyn. 36 (5), 591–613.

Zhao, Z., Jiang, F., Wu, X., Wang, S., Qiao, Y., Liu, K., Wang, S., 2006. Sanmenxia Loess and Paleoenvironmental Change. J. China Univ. Geosci. 17, 283–290.

Zhu, W., Wu, C., Wang, J., Zhou, T., Li, J., Zhang, C., Li, L., 2017. Heavy mineral compositions and zircon U-Pb ages of Cenozoic sandstones in the SW Qaidam basin, northern Tibetan Plateau: Implications for provenance and tectonic setting. J. Asian Earth Sci. 146, 233–250.

Zhu, Z., 1989. The formation of terraces in the middle reach of the Yellow River and the drainage system evolution. Acta Geographica Sin. 61 (4), 429–440 (in Chinese with English abstract).